

Vibrationally-resolved Charge Transfer of O^{3+} with Molecular Hydrogen

J. G. Wang* and P. C. Stancil†

*Department of Physics and Astronomy and the Center for Simulation Physics
The University of Georgia, Athens, GA, 30602-2451, USA*

A. R. Turner‡ and D. L. Cooper§

Department of Chemistry, University of Liverpool, Liverpool L69 7ZD, UK

Abstract

Charge transfer due to collisions of ground state $O^{3+}(2s^22p^2P^o)$ ions with molecular hydrogen are investigated using the quantum-mechanical molecular-orbital (QMO) coupled-channel method. The QMO calculations utilize *ab initio* adiabatic potentials and nonadiabatic radial coupling matrix elements obtained with the spin-coupled valence-bond approach for a representative range of orientation angles and diatom internuclear separations. Vibrationally-resolved cross sections for nondissociative single electron capture are obtained for energies between 0.1 eV/u and 10 keV/u for H_2 in its ground vibrational level using the infinite order sudden approximation (IOSA). Two further approximations are considered in which the electronic radial couplings are assumed to be independent of the diatom stretching. In the first case, vibrational motion is taken into account by multiplying the electronic radial couplings by Franck-Condon (FC) ionization factors while in the second, vibrational motion is completely neglected. We refer to these two approaches as the vibrational sudden approximation (VSA) and the electronic approximation (EA), respectively. In the latter, the resulting cross sections for electronic transitions are multiplied by FC factors to obtain relative vibrationally-resolved cross sections which are independent of the collision energy (the centroid approximation). Comparison with existing experimental data for total and electronic state-selective cross sections shows best agreement with IOSA and VSA, but discrepancies for EA. The triplet-singlet electronic cross section ratio reveals a departure at low collision energies from the statistical value.

PACS numbers: 34.70.+e, 82.30.Fi, 34.50.-s, 34.20.Mj

*Present address: Institute of Applied Physics and Computational Mathematics, P. O. Box 8009, Beijing 100089, P. R. China; Electronic address: wang_jianguo@iapcm.ac.cn

†Electronic address: stancil@physast.uga.edu

‡Present address: Department of Chemistry, University of Edinburgh, West Mains Road, Edinburgh EH9 3JJ, UK; Electronic address: Andrew.Turner@ed.ac.uk

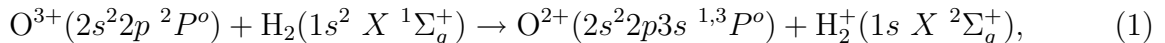
§Electronic address: dlc@liv.ac.uk

I. INTRODUCTION

Electron capture by multiply charged ions colliding with H_2 is an important process in laboratory and astrophysical plasmas. It provides a recombination mechanism for multiply charged ions in astronomical environments ionized by x-rays, so-called x-ray dominated regions (XDRs) [1]. In XDRs, x-rays are preferentially absorbed by heavy elements in inner shell transitions leading to the production of multiply charged ions in spatial co-existence with neutral H, H_2 , and He. The multiply charged ions are thought to be converted to singly charged ions through rapid charge exchange with the neutral species. However, for a large range of the ionization parameter (x-ray ionization rate divided by the gas number density), the electron and H abundances are sparse [2], leaving only H_2 and He to participate in charge exchange. For some ions, such as C^{2+} and S^{2+} , charge transfer may proceed slowly. These ions may therefore be signatures of XDRs [3]. In laboratory plasmas, such as the divertor region of a tokamak fusion device, charge exchange of impurity ions with H_2 plays an important role in the ionization balance and the production of radiative energy loss leading to plasma cooling [4]. Recently, it has been found that ion-molecule charge transfer processes are of particular significance for extreme ultraviolet (EUV) and x-ray emission from comets and from planetary atmospheres. Soft x-ray emission has been observed from many comets, including comet Hale-Bopp [5] and comet Hyakutake [6, 7]. It has been suggested that these EUV/x-ray emissions result from charge transfer of highly-charged solar wind ions (e.g., O^{q+} , C^{q+} and Ne^{q+}) with cometary neutral species including H_2O , its dissociation products H, H_2 , O, and OH, and CO and CO_2 [8, 9]. Indeed, recent analysis of EUV/x-ray *Extreme Ultraviolet Explorer* spectra of comet Hyakutake [10] has revealed emission lines from multiply charged ions (O^{4-6+} , $\text{C}^{4,5+}$, and Ne^{7+}). A broad line in *Chandra X-ray Observatory* (*CXO*) observations of comet Linear S4 [11] appears to be attributable to O^{5+} , and emission lines due to many highly charged ions including O^{6+} and O^{7+} have been detected in comet McNaught-Hartley by the *CXO* [12]. These observations provide strong evidence for the charge transfer mechanism for EUV/x-ray emission from comets. In a similar way, observed x-ray emission from the Jovian aurora is thought to be driven by charge transfer in collisions of multiply charged oxygen and sulfur, and possibly sodium and carbon, ions with the atmospheric neutrals H, He, and H_2 [13, 14]. The oxygen, sulfur, and sodium ions are thought to be Iogenic and are accelerated into the Jovian atmosphere along closed magnetic

field lines connecting the Jovian pole to the outer Io plasma torus. The carbon is believed to be provided by the solar wind. In order to model and understand the behavior of these environments, it is necessary to obtain total, electronic state-selective (ESS), and vibrational (or even rotational) state-selective (VSS) electron capture cross sections for collisions of multiply charged ions with molecules. While there have been numerous experimental investigations of total cross sections and rates coefficients, state-selective studies are sparse. Such collision systems have received little theoretical attention due to the increase in the degrees of freedom compared to typical ion-atom studies. However, some molecular-orbital (MO) treatments have been attempted (e.g., Be⁴⁺ [15], B³⁺ [16], C²⁺ [17], C⁴⁺ [18]) for collisions with H₂ though within the semiclassical MO (SCMO) impact parameter formalism. We are only aware of one work to date which has performed a quantum-mechanical scattering calculation for a multiply-charged ion, that of N²⁺ with H₂ [19].

In this paper we extend the available studies on multiply-charged ion-molecule collisions by investigating the reaction



using the quantum-mechanical molecular-orbital (QMO) coupled-channel method. In the QMO calculations, *ab initio* adiabatic potentials and nonadiabatic radial coupling matrix elements are incorporated, for various orientations θ , defined as the angle between the H-H diatom nuclear vector \mathbf{r} and the internuclear radius vector from the H₂ center of mass to the oxygen ion \mathbf{R} (*i.e.*, *Jacobian coordinates*), and for various r separations. The molecular data were obtained for $R = 3 - 13 a_0$, $r = 1.2, 1.4, 1.6, \text{ and } 2.0 a_0$, and $\theta = 25^\circ, 45^\circ, \text{ and } 89^\circ$ with the spin-coupled valence-bond (SCVB) approach. This range of molecular data allows for investigations of reaction (1) at a variety of approximations including total and electronic state-selective cross sections with the electronic approximation (EA) which neglects vibrational motion, and vibrationally-resolved cross sections with the infinite order sudden approximation (IOSA), vibrational sudden approximation (VSA), and centroid approximation (CA).

Numerous experimental studies have been performed for reaction (1). The group at Oak Ridge National Laboratory (ORNL) [20–23] measured the total single charge transfer cross section from 42 eV/u to 10 keV/u. Afrosimov *et al.* [24] obtained a total cross section at 0.8 keV/u of $1.8 \times 10^{-16} \text{ cm}^2$, which is about twice the cross section measured by the ORNL

group. Church and Holzscheiter [25] measured the total electron capture rate coefficient at 1500 K in a Penning trap, though without knowledge of the product channels. More recently, two new measurements were made, one being the total single electron capture (SEC) and ESS cross sections between 45 and 752 eV/u by Beijers *et al.* [26] via photon emission spectroscopy (PES) and the other, total single charge transfer cross sections between 0.2 and 200 eV/u [27]. In general, there are some significant divergences among the measurements, especially for the comparison of the cross sections of Okuno *et al.* [27] with the other results. To date this collision system has not been investigated theoretically and we are unaware of any VSS cross section measurements.

Section II describes the molecular potential and coupling data utilized in the QMO calculations, while section III discusses the scattering calculation approach. Section IV presents the results of the scattering calculations including comparisons of total and state-selective cross sections and rate coefficients with experiments, while section V briefly gives a summary of the work. Atomic units are used throughout unless otherwise noted.

II. ELECTRONIC STRUCTURE CALCULATIONS

The adiabatic potential energy curves and nonadiabatic radial couplings were obtained using the SCVB method (see for example Cooper *et al.* [28] and Turner [29]). This is a fully flexible *ab initio* technique and, as such, we expect the molecular region to be described with much the same accuracy as the asymptotic separated-atom limit. As this is the first triatomic charge transfer system that has been studied in detail using the SCVB approach it was decided to treat just a limited number of states of ${}^2A'$ symmetry. Estimation of the avoided crossing distances from the experimental values of the energy separations of the O^{2+} states indicated that charge transfer to the $2p3s\ {}^1,3P^o$ channels should be the most important processes at the collision energies of interest. Therefore, only capture to the $O^{2+}(2p3s\ {}^1,3P^o)$ states was investigated.

All calculations were performed using the C_s point group and only states of ${}^2A'$ molecular symmetry were considered. Geometries with $\theta = 0^\circ$ and $\theta = 90^\circ$ were not considered, so as to avoid potential problems from the change of point group. We adopted a Dunning correlation-consistent basis set of quintuple- ζ quality for O/H consisting of $(14s8p4d3f)/(8s4p3d)$ Cartesian Gaussian type orbitals generally contracted to $[6s5p4d3f]/[5s4p3d]$. This set was aug-

mented by two diffuse, even-tempered basis functions on oxygen, one s -type function and one p -type function. The oxygen core electrons ($1s^2$) were assumed to have little or no effect on the charge transfer process and so they were accommodated in appropriate orthogonal natural orbitals taken from a state-averaged multiconfiguration self-consistent-field (MCSCF) calculation on triplet atomic O^{2+} . The five valence electrons were accommodated in five one-electron nonorthogonal spin-coupled orbitals that, when converged, took the following asymptotic characters: $\phi_1 \approx O^{2+}(2s)$, $\phi_2 \approx H_2^+(1\sigma_g)$, $\phi_3 \approx O^{2+}(2s')$, $\phi_4 \approx O^{2+}(2p_x)$, and $\phi_5 \approx O^{2+}(2p_z)$. The forms of the orbitals were found to be maintained over the whole range of nuclear geometries. These forms are easily determined by examining the orbital coefficients. A total of 18 virtual orbitals were selected from the virtuals generated from the spin-coupled calculation and these are listed according to their asymptotic characters in Table I. In addition to these virtual orbitals, two natural orbitals taken from a MCSCF calculation on the neutral H_2 were imported into stack 2 (see Table I), to aid in the description of the entrance channel.

The configuration list for the SCVB expansions was generated by performing all single and double vertical excitations along with singly ionic excitations (that produced a configuration of the correct symmetry) from the spin-coupled configuration, from the dominant configuration of each $2p3s(^{1,3}P^o)$ and $2p3p(^{1,3}P, ^3D, ^3S)$ excited state and from the dominant configuration of the charge-transfer state. The dominant configuration of a state was found to correspond directly to its asymptotic character. Additional selected excitations to the imported orbitals were also included. This scheme generated just 423 spatial configurations (1707 symmetry-adapted VB structures). Table II gives a comparison of our values of the asymptotic energy separations with the experimental values. Energy separations for the $2p3p$ channels are also listed even though only capture to the $2p3s$ channels are considered here. The calculation for comparison with experimental values was performed with $R = 25 a_o$, $r = 1.4 a_o$, and $\theta = 89^\circ$. At first sight, agreement with the experimental values was found to be reasonable for all of the channels. However, only after completing all of the scattering calculations did we realize that we had compared the calculated asymptotes with an incorrect “experimental” value for the ionization energy of H_2 , because we had failed to distinguish properly between the vertical and adiabatic values of that quantity. As such, the asymptotic energies are not as good as we had first supposed, with an error in the entrance channel that exceeds 1 eV. However, with the asymptotic energies shifted to

match experiment for the $1\ ^2A'$ channel, the maximum deviation from experiment for the remaining capture channels is 0.11 eV, that being for the $2p3p\ ^3P$ channel. The agreement for the $2p3s$ channels is satisfactory with the largest deviation being just 0.03 eV, in the case of the $2p3s\ ^1P^o$. The source of the corresponding deficiency in the spin-coupled VB expansion has since been identified, and is well understood. The scattering calculations had in fact already been carried out, before this problem was detected, with diabats that had been shifted so as to match exactly the correct asymptotic experimental values (see below, and in particular, eq. 8), so that the problem is alleviated to a large extent. Although the positions, magnitudes and widths of the adiabatic couplings will not have been described as well as in our previous work on diatomic charge transfer systems (for example [31]), we do expect to reproduce the qualitative trends of the charge transfer process reasonably well and we are able also to compare different approximations for dealing with the vibrational motion. Of course we would not expect our final cross sections to have the same quantitative accuracy as in our previous studies of this type. Improvements to the SCVB calculations are currently being pursued. New scattering calculations will be performed when they are completed to test the effect, if any, of the improved SCVB representation.

We are interested in what effect variations of the geometric parameters might have on the avoided crossing distances and on the forms of the radial couplings. First, the variation with respect to the angle θ is considered. The potential energy curves for the geometries $r = 1.4\ a_0$ (equilibrium bond length) and $\theta = 25^\circ, 45^\circ, 89^\circ$ are shown in Fig. 1(a) and the corresponding nonadiabatic radial couplings are shown in Fig. 1(b). The avoided crossing distances (with respect to R) and energy separations between the adiabatic potential energy curves (for all collision symmetries) are listed in Table III. From the potential energy curves and the avoided crossing data, one can see that the two key avoided crossings occur at practically the same internuclear distance R for all three angles, and with fairly constant energy differences. This suggests that the angle of approach should have a small effect on the characteristics of the electron capture to these channels, at least for this value of r . A similar lack of significant θ sensitivity was noted for other multiply-charged ion- H_2 studies [16, 18, 32]. However, the corresponding radial couplings show some variation in the height of the peaks, though all of the peaks occur at very similar R . If they are used to calculate capture cross sections, such as through pure electronic transitions (EA, see below) or EA with Franck-Condon factors, one would expect the results for all three angles, and any

others, to be fairly similar based on the close similarity of the potentials, but this conclusion appears to be modified as a result of the variation in the radial couplings as will be seen below.

The dependence of the potential energy curves on the H-H bond length (r) was also investigated. The angle θ was kept constant at 89° while R and r were varied. The potential energy curves with respect to R for the geometries $\theta = 89^\circ$ and $r = 1.2, 1.4, 1.6,$ and $2.0 a_0$ are shown in Fig. 2 and the corresponding nonadiabatic radial couplings are illustrated in Fig. 3. These values are chosen to encompass the equilibrium bond length of H_2 and to provide both larger and smaller values for use in averaging over the H_2 and H_2^+ vibrational wave functions. We also calculated the potential energy curves and radial couplings for the geometries $\theta = 45^\circ$ and $r = 1.2, 1.4,$ and $1.6 a_0$ (not shown). It is obvious from the potential energy curves and the avoided crossing data (Table III) that the variation of the H-H bond length has a profound effect on the collision internuclear distances R at which the avoided crossings occur. As the bond length increases, both avoided crossings occur at consecutively smaller and smaller values of R and, as a consequence, the energy gaps between the adiabatic potentials also increase. The corresponding radial coupling peaks also shift and, more significantly, change character from sharper to broader profiles as the distance of the avoided crossings decrease and the energy gaps increase. This should have a large effect on the state-selective (and thus the total) charge transfer cross sections.

III. SCATTERING THEORY

The cross sections for ion-molecule nondissociative SEC are calculated in this work in a QMO formalism which follows closely that for ion-atom collisions described thoroughly in the literature [33, 34], but adapted for molecular targets following Sidis [35] as previously outlined by Stancil *et al.* [19].

The ion-diatom collision system can be represented by the Hamiltonian

$$H(\mathbf{R}, \mathbf{r}, \rho_i) = -\frac{1}{2\mu_R} \nabla_R^2 - \frac{1}{2\mu_r} \nabla_r^2 + H_{\text{ad}}(\rho_i | \mathbf{R}, \mathbf{r}) \quad (2)$$

where ρ_i is the electronic coordinate, μ_R the collision system reduced mass, μ_r the H_2 reduced mass, and H_{ad} the adiabatic electronic Hamiltonian of the triatomic molecular ion.

The Schrödinger equation for the adiabatic Hamiltonian is then

$$H_{\text{ad}}(\rho_i|\mathbf{R}, \mathbf{r})\phi_\gamma(\rho_i|\mathbf{R}, \mathbf{r}) = \varepsilon_\gamma(R, r, \theta)\phi_\gamma(\rho_i|\mathbf{R}, \mathbf{r}) \quad (3)$$

where $\varepsilon_\gamma(R, r, \theta)$ and $\phi_\gamma(\rho_i|\mathbf{R}, \mathbf{r})$ are the triatomic adiabatic electronic energy and wave function, respectively for electronic state γ . The total wave function for the ion-molecule system in the perturbed stationary-state (PSS) approximation is

$$\psi(\mathbf{R}, \mathbf{r}, \rho_i) = \sum_\gamma N_\gamma(\mathbf{R}, \mathbf{r})\phi_\gamma(\rho_i|\mathbf{R}, \mathbf{r}) \quad (4)$$

where N_γ is the electronic scattering amplitude.

The lowest level of approximation which will be considered in this work is obtained by fixing r and θ and computing the cross section following standard ion-atom QMO methods. Typically, one sets r equal to the equilibrium nuclear separation r_e (1.4 a_0 for H_2) and $\theta = 0^\circ$ for a collinear geometry, though we chose other angles in this work. As discussed above, the results are not expected to be very sensitive to the adopted value of θ for the case of multiply-charged incident ions, but a significant steric effect is expected for singly-charged ions (e.g. [36]). This approximation is essentially equivalent to the approaches of Gargaud and McCarrol [37], Kimura and Lane [38], Saha *et al.* [39], and Kravis *et al.* [40], for example, except that in this earlier body of work the interactions were described using model potentials for an ion-“atom” collision and adopting the H_2 adiabatic ionization energy. While in this work, consideration of the ion-molecule potential surfaces, gives the H_2 vertical ionization energy. Nevertheless, this approximation results in purely electronic transitions and we refer to it as the electronic approximation (EA). The method is expected to give reasonable total cross sections, $\sigma_{\gamma,\gamma'}^{EA}$, for energies greater than ~ 100 eV/u.

The highest level of approximation that we consider here involves expanding N_γ over a basis of vibrational states v

$$N_\gamma(\mathbf{R}, \mathbf{r}) = \sum_v F_{\gamma v}(\mathbf{R})\chi_{\gamma v}(\mathbf{r}) \quad (5)$$

where $\chi_{\gamma v}(\mathbf{r})$ are the vibrational wave functions of the diatom, either H_2 or H_2^+ , and the rotational quantum number J of the diatom is taken to be zero. Following Sidis [35], insertion of Eqs. (2), (4), and (5) into the Schrödinger equation, gives the PSS scattering equation in the diabatic representation

$$\{\nabla_R^2 + 2\mu_R[E - \varepsilon_{\gamma v}^d(R, \theta)]\}F_{\gamma v}(R, \theta)$$

$$= 2\mu_R \sum_{\gamma' \neq \gamma} \sum_{v'} V_{\gamma v, \gamma' v'}^d F_{\gamma' v'}(R, \theta) \quad (6)$$

with the vibrationally-resolved diabatic potential coupling given by

$$V_{\gamma v, \gamma' v'}^d(R, \theta) = \langle \chi_{\gamma v}(r) | V_{\gamma, \gamma'}^d(R, r, \theta) | \chi_{\gamma' v'}(r) \rangle, \quad (7)$$

the brackets referring to integration over r , $V_{\gamma, \gamma'}^d(R, r, \theta)$ the electronic diabatic potential coupling, and $\varepsilon_{\gamma v}^d(R, \theta)$ the diabatic vibronic potential which we take to be given by

$$\varepsilon_{\gamma v}^d(R, \theta) = \varepsilon_{\gamma}^d(R, r_e, \theta) + \Delta\varepsilon_{\gamma} + \varepsilon_{\gamma v}. \quad (8)$$

$\varepsilon_{\gamma v}$ is the pure, unperturbed vibrational excitation energy of of the diatom. $\varepsilon_{\gamma}^d(R, r, \theta)$ and $V_{\gamma, \gamma'}^d(R, r, \theta)$ are obtained by a unitary transformation from the adiabatic to the diabatic representation [34, 41] parameterized for r and θ using the adiabatic molecular data given in section II. $\Delta\varepsilon_{\gamma}$ is a shift applied to the electronic diabatic energies to ensure exact agreement in the separated-atom asymptotic limit, as $R \rightarrow \infty$, with experiment (see Table II), thereby providing a means to correct errors in the *ab initio* potentials as discussed in Section II. We only consider $\text{H}_2(v=0)$ as the experimental conditions are such that H_2 is presumed to be in the vibrational ground state. The integration over r in Eq. (7) is performed between $r = 1.0 \text{ a}_0$ and $r = 2.0 \text{ a}_0$ which accounts for the vast majority ($> 99\%$) of the area under the $\text{H}_2(v=0)$ vibrational wave function. Due to the limited number of r -values calculated in Section II, third-order spline interpolation and linear extrapolation is used.

In Fig. 4, the vibronic energies $\varepsilon_{\gamma v}^d(R, \theta)$ are presented. The two final electronic capture channels are resolved into ten vibrationally excited states of $\text{H}_2^+(v' = 0, 1, 2, \dots, 9)$ each, while only $\text{H}_2(v=0)$ is considered for the initial channel. Within a given final electronic channel, the crossing distance increases with v' . If the crossing distance for the vibrational ground state is small ($< 5 \text{ a}_0$), the vibrationally-resolved cross sections are expected to increase with v' since the crossing distances for the excited states may fall into an intermediate range (say $6 - 10 \text{ a}_0$) which is optimal for efficient charge transfer probabilities. Conversely, if the crossing distance for the vibrational ground state of H_2^+ is large, the vibrationally-resolved cross sections will decrease with v' as the diabaticity of the interaction increases. The latter situation represents the current collision system as the electronic crossings are greater than 8 a_0 . In Fig. 4, we note that the vibronic energies for $1 \text{ } ^2A'$ with $v' \geq 3$ overlap the $2 \text{ } ^2A'$ vibronic energies. Some swapping of probabilities may occur between these channels, particularly those which are quasi-resonant.

The vibronic diabatic radial couplings $V_{\gamma v, \gamma' v'}^d(R, \theta)$ are illustrated in Fig. 5. The absolute values of vibronic radial couplings are smaller than the purely electronic radial couplings. The couplings for $v' = 2$ and 3 into the $2p3s^3P^o$ channel are the largest. As a consequence, VSS cross sections to these states are expected to be the most important, though the locations of crossings also play a significant role.

The above description is our implementation of the so-called infinite order sudden approximation (IOSA) which is appropriate when the rotational periods are much longer than the collisional time [35]. Following a partial-wave decomposition of F_γ , Eq. 6 can be used to obtain VSS cross sections $\sigma_{\gamma v, \gamma' v'}^{IOSA}$ for different orientations θ which are expected to be reliable for energies greater than ~ 0.1 eV/u.

If the collisional time scale is much shorter than the vibrational period or the diabatic coupling is a weak function of r , a Franck-Condon (FC) type approximation can be made for the diabatic couplings giving

$$\langle \chi_{\gamma v} | V_{\gamma, \gamma'}^d(R, r, \theta) | \chi_{\gamma' v'} \rangle \rightarrow V_{\gamma, \gamma'}^d(R, \theta) \langle \chi_{\gamma v} | \chi_{\gamma' v'} \rangle \quad (9)$$

where $\langle \chi_{\gamma v} | \chi_{\gamma' v'} \rangle$ is the square-root of the FC ionization factor for the overlap of the H_2 and H_2^+ vibrational wave functions. In Fig. 5, these FC-type vibrationally-resolved diabatic radial couplings are plotted in comparison to those obtained with equation (7), the former being larger for the 1 – 3 diabatic coupling. This approximation can also be used to compute VSS cross sections $\sigma_{\gamma v, \gamma' v'}^{VSA}$. It may be applicable for $E > 50$ eV/u and we refer to it as the vibrational sudden approximation (VSA). An alternative approximation, the centroid approximation (CA), can give a VSS cross section by merely multiplying the EA cross section by a FC factor

$$\sigma_{\gamma v, \gamma' v'}^{CA} = \sigma_{\gamma, \gamma'}^{EA} |\langle \chi_{\gamma v} | \chi_{\gamma' v'} \rangle|^2. \quad (10)$$

We note that the CA and VSA are not equivalent. The FC ionization factors would imply that the dominant VSS cross section would be for capture into $\text{H}_2^+(v' = 2)$ followed by $v' = 1, 3, 4, 0, \dots$, independent of collision energy. A similar discussion for the various approximations has been previously given within a semiclassical impact-parameter picture [42, 43].

Finally, as the scattering calculations are performed for a fixed orientation angle, the

orientation-averaged cross sections are obtained in the usual way [35]:

$$\begin{aligned}\sigma &= \frac{1}{4\pi} \int_0^{2\pi} d\phi \int_0^\pi \sigma(\theta) \sin\theta d\theta \\ &= \int_0^{\pi/2} \sigma(\theta) \sin\theta d\theta.\end{aligned}\tag{11}$$

IV. RESULTS AND DISCUSSION

Total and state-selective cross sections [51] have been obtained for the three approximations discussed in the previous section: (i) EA, (ii) VSA, and (iii) IOSA, with vibrational motion being unaccounted for in the first method. In order to ensure convergence for the total and ESS cross sections, calculations for IOSA and VSA were performed with the maximum vibrational quantum numbers $v'_{\max}=4, 7,$ and 9 . The convergence study suggests that vibrational states with $v'_{\max} > 9$ should contribute less than 5% to the total and ESS cross sections for the considered energy range. The results presented here were all obtained with $v'_{\max} = 9$.

A. Total Cross Sections

In Figs. 6a-d orientation-dependent total cross sections $\sigma(\theta)$ are displayed for the collisional energies of 0.1 eV/u to 10 keV/u. The differences due to the orientation for an individual approximation is typically less than a factor of two, and it is typically less than the differences between various approximations. While the differences between IOSA, VSA, and EA are expected, and in fact EA should not be applied below ~ 100 eV/u, the orientation variance within EA and IOSA was not expected due to the near isotropy of the potential surfaces. However, the orientation variation in the radial couplings noted in section II is probably responsible for this effect and suggests that orientation isotropy should be assumed with caution.

In Fig. 7, the orientation-averaged total cross sections are compared to the available measurements. For low collision energies ($\lesssim 0.5 - 5$ eV/u), the cross sections obtained with all of the methods generally display the typical Langevin $E^{-1/2}$ behavior. For $E \gtrsim 1$ eV/u, the EA cross section decreases smoothly with collision energy, while the IOSA and VSA cross sections decrease somewhat more rapidly. At about 100 eV/u, the IOSA cross section reaches

a local minimum, and remains relatively flat at higher energies. As shown in Fig. 4, channels which include vibrationally excited states v' of H_2^+ have longer diabatic crossing distances than for $v' = 0$. As most of the crossing distances for vibrationally excited states are at large distances ($R_x > 8a_0$), the differences in the behavior of the low-energy cross sections of IOSA and VSA with that of EA are expected. The VSA radial couplings shown in Fig. 5 for $\text{O}^{2+}(2p3s\ ^3P^o)+\text{H}_2^+(v')$ vary by factors of ~ 0.5 -2 compared to the IOSA couplings. This difference is responsible for the discrepancies, though relatively small, between the IOSA and VSA cross sections.

For the collisional energy range $0.3 \leq E \leq 200$ eV/u, the present EA cross sections are in surprisingly good agreement with the measurements of Okuno *et al.* [27], though this is probably fortuitous as the EA method is not expected to be reliable in this energy regime. The VSA result is also in agreement with Okuno *et al.*, but is smaller by a factor of ~ 1.5 for $E > 10$ eV/u. Conversely, the IOSA cross section, the result which would be expected to be the most accurate, is smaller than the Okuno *et al.* measurement at all energies except for the one experimental point at 0.3 eV/u. The oscillation in the Okuno *et al.* result between 10 and 20 eV/u is not present in any of our calculations. At the lowest energies, $E < 0.3$ eV/u, only two measurements are available, one estimated from the rate coefficient measured by Church and Holzschleiter [25] at 0.134 eV/u and the other from Okuno *et al.* [27] at 0.21 eV/u. The cross section for the first is estimated to be $1.4 \pm 0.14 \times 10^{-14}$ cm², while the latter is $1.1 \pm 0.28 \times 10^{-15}$ cm². The current calculations lie between these measurements with a range of $5 - 8 \times 10^{-15}$ cm² being closer to the Church and Holzschleiter result. The Okuno *et al.* result is questionable as it involves a factor of 4.4 drop in the cross section when going from 0.38 to 0.21 eV/u. On the other hand, the Church and Holzschleiter value is about three times larger than the IOSA cross section. However, this experimental value, and in fact all of the available measurements except that of Beijers *et al.* [26], is not a pure SEC measurement. It is an ion loss measurement and so includes contributions from two-electron processes: true double capture (TDC), transfer ionization (TI), and autoionization following double capture (ADC). All of the experiments which measured the total cross section obtained the sum of SEC, TI, and ADC, referred to as $q, q - 1$. Okuno *et al.* also measured TDC (or $q, q - 2$) and found it to be between $\sim 5 - 17\%$ of $q, q - 1$ with the percentage increasing with collision energy from 0.21 to 188 eV/u. We are unaware of any experimental data for ADC or TI for this system, but a classical trajectory Monte Carlo

(CTMC) calculation at 10 keV/u by Wang *et al.* [45] finds them to be 17% and $< 1\%$ of $q, q - 1$, respectively. Further, the Wang *et al.* [45] CTMC calculation finds that TDC is 16% of $q, q - 1$. Typically, TI decreases rapidly with decreasing collision energy, while ADC may rise somewhat. Therefore, it is likely that less than $\sim 80\%$ and $\sim 85\%$ of the Church and Holzscheiter [25] and Okuno *et al.* [27] measurements, respectively are SEC, improving the agreement with the current IOSA calculations.

For higher energies, $40 \leq E \leq 50,000$ eV/u, a number of experimental results are available, but in some cases differing by factors of 2-3 and with the divergence increasing with decreasing energy. The $q, q - 1$ results of Okuno *et al.* [27], Afrosimov *et al.* [24], and Phaneuf *et al.* [23], for energies between 60 eV/u and 200 eV/u, fall between the EA and VSA calculations. The IOSA and VSA results are in good agreement with the SEC measurements of Beijers *et al.* [26] and the $q, q - 1$ measurements of Crandall *et al.* [20] and Phaneuf *et al.* [23] for $E > 250$ eV/u.

Concerning the results of Beijers *et al.* [26], photon energy spectroscopy (PES) of the product ions was used to determine absolute state-selective cross sections. In principle, if the emission from the dominant capture channels could be measured, then the total cross section could be obtained from the sum of the state-selective cross sections. However, only a portion of the transitions could be measured due to the limited wavelength window of the detector. Generally, the emission cross sections have contributions due to cascades from capture to higher-lying states. Therefore, state-selective cross sections are inferred from the measured emission cross sections, but corrected for cascades using transition probability branching ratios. However, in our study of $O^{3+} + H$ [31], we found that the adopted branching ratios were not consistent when compared with a critical compilation [46] which resulted in corrections of about 30%-50%. This translated into enhancements of 30%-100% for the $O^{3+} + H$ cross sections. For capture from H_2 , cascade effects are negligible so that corrections due to the branching ratios are not relevant (at least for the $2p3s \ ^1P^o$, see further discussion below). However, the total cross sections reported by Beijers *et al.* [26] include contributions due to capture to the $2p3p$ configuration, but as discussed in Wang *et al.* [31] these states are not populated in collisions with ground state O^{3+} , but rather via metastable O^{3+} collisions. Therefore, the total cross sections of Beijers *et al.* shown in Fig. 7 might be overestimated by about 50% (see below).

B. Electronic State-selective Cross Sections

State-selective cross sections for capture to $O^{2+}(2p3s\ ^1P^o)$ and $O^{2+}(2p3s\ ^3P^o)$ are shown in Fig. 8. In the energy regime $E < 1$ eV/u, capture to $O^{2+}(2p3s\ ^1P^o)$ dominates according to the EA results. However, with increasing energy, capture to $O^{2+}(2p3s\ ^3P^o)$ becomes important ultimately dominating over capture to $O^{2+}(2p3s\ ^1P^o)$ for $E > 2$ eV/u. Conversely, if either IOSA or VSA are applied, capture to $O^{2+}(2p3s\ ^3P^o)$ dominates over the entire energy range considered. The inclusion of vibrational motion in the VSA and IOSA results in diabatic crossings shifted to larger internuclear distances and thereby reductions in the cross sections, with the $2s3p\ ^1P^o$ being the most affected. Comparing the IOSA and VSA results, the electronic state-selective cross sections are very similar. However, the VSA cross section for capture to $O^{2+}(2p3s\ ^3P^o)$ is about 40% larger than that of the IOSA result for $E < 10$ eV/u. This is a consequence of the similarity of the vibrationally-resolved radial couplings for $O^{2+}(2p3s\ ^1P^o)$ with IOSA and VSA as shown in Fig. 5. However, the VSA $O^{2+}(2p3s\ ^3P^o)$ radial couplings are somewhat larger than the IOSA couplings.

Absolute electronic state-selective cross section measurements, at the LS level, have been performed with the PES method, as mentioned above, for $O^{2+}(2p3s\ ^1P^o, ^3P^o; 2p3p\ ^3S, ^3P, ^3D)$ [26]. For capture to $2p3s\ ^1P^o$, the IOSA and VSA cross sections are in good agreement with the experiment though somewhat larger. For $2p3s\ ^3P^o$, the IOSA and VSA cross sections, for $E < 200$ eV/u are about a factor of two larger than the results of Beijer *et al.*. For higher energies, the agreement is worst. Large discrepancies exist for the EA cross sections, all being significantly larger than the measurements. This is consistent with the differences in the total cross sections.

The current results generally confirm the importance of including the vibrational motion in the scattering calculation via either the IOSA or, surprisingly, the VSA methods. The EA method is unreliable even at the highest energies. However, two considerations should be noted concerning the results of Beijers *et al.* [26] as discussed by Wang *et al.* [31]: (i) the use of inaccurate transition probability data and (ii) metastable contamination of the ion beam. The first affects the magnitudes of the inferred ESS cross sections while the latter suggests that some fraction of the measured ESS cross section, or its entirety, may be due to capture from an O^{3+} metastable state and not the ground state. For example, Beijers *et al.* find that the cross sections for capture to $2p3p\ ^3P$ and 3D are comparable to cross

sections for $2p3s\ ^1P^o$ and $^3P^o$ capture. However, for collisions with ground state O^{3+} the $2p3p\ ^3P$, 3D capture channels are found to be diabatic with avoided-crossing distances of ~ 20 and $\sim 18\ a_0$, respectively [29]. Examination of the OH_2^{3+} potential surfaces as given in Figs. 1 and 2, reveal no short-range, endoergic avoided-crossings for $R \gtrsim 5$ indicating that possible crossings would have effective thresholds of at least 7 eV/u. This suggests, contrary to the PES measurements, that state-selective cross sections for capture to the $2p3p$ configuration should be small. On the other hand, avoided-crossings for the $2p3s$ states are in optimal locations between $R_x \sim 8-11\ a_0$ indicating significant cross sections as found by the current calculations.

Beijers *et al.* [26] estimated a 12% metastable contamination in the oxygen ion beam. Considering the possibility of a significant metastable population, Wang *et al.* [31] estimated what contribution it might make to the PES spectra. Given that the metastable is a quartet, the singlets (i.e., the $2p3s\ ^1P^o$) are mostly unaffected by the presence of the metastable. They concluded that the PES measurements for the triplet $2p3p$ states for the neutral H_2 beam is due to the O^{3+} metastable via either direct charge transfer or cascade from the $2p3d$ and $2p4s$ states with little contribution from the O^{3+} ground state. Therefore, the $2p3p$ state-selective cross sections should not be added to those of the $2p3s$ to give the total cross section. In this regard, the total cross sections given by Beijers *et al.* are likely overestimated. On the other hand, the experimental state-selective cross sections for the $2p3s$ states may be underestimated. While the PES signal due to the $2p3s\ ^3P^o$ is affected by cascades resulting from capture due to the metastable, the contribution is probably small compared to direct capture from the ground state. However, Beijers *et al.* mistakenly corrected the $2p3s\ ^3P^o$ cross sections by subtracting what they took to be the cascade component due to capture to the $2p3p$ states from the ground state O^{3+} . In fact, Wang *et al.* [31] argued that the $2p3p$ emission cross sections are due to capture from a metastable O^{3+} state and therefore should not be subtracted from the $2p3s\ ^3P^o$ emission cross section. Further, since the $2p3s\ ^1P^o$ appears to be little affected by cascades, from the ground or metastable states, the discrepancy with the current calculations may be due to a larger metastable fraction than estimated by Beijers *et al.*. Increasing the metastable contamination to $\sim 30\%$ would bring the current IOSA and VSA calculations into reasonable agreement with the measurements. Further measurements and calculations are needed to clarify this possibility.

Finally, in some astrophysical models, in particular that due to x-ray emission following

charge transfer [47–49], the resulting population within triplet and singlet states is assumed to be according to spin statistics (i.e., 3:1) because of the lack of experimental and theoretical data. Ratios of triplet to singlet cross sections for $O^{3+} + H_2$ are plotted in Fig. 9. Significant departures from statistical equilibrium are found for all energies considered. In particular, the ratio for the IOSA results is always greater than ~ 4 . The measurements of Beijers *et al.* [26] are consistent with the equilibrium value, but the uncertainties are large. However, if the measured cross sections for the $2p3s\ ^3P^o$ are too small as argued above, their correction might bring the measured ratio into agreement with the IOSA calculation.

C. Vibrationally-resolved Cross Sections

Figs. 10 and 11 display vibrationally-resolved cross sections for capture to $O^{2+}(2p3s\ ^1P^o)$ and $O^{2+}(2p3s\ ^3P^o)$, respectively obtained with the IOSA method. It can be seen that the ordering of the cross sections as a function of $H_2^+(v')$ varies somewhat with collision energy, but that capture to small v' dominates. Further, the total cross section is converged as the v' -resolved cross sections decrease with increasing v' . This behavior is related to both the increase in diabatic crossing distance and decrease of the radial coupling strength with increasing v' . Figs. 12 and 13 display the v' -distribution for capture to $O^{2+}(2p3s\ ^1P^o)$ and $O^{2+}(2p3s\ ^3P^o)$, respectively at 1 eV/u and 100 eV/u for IOSA, VSA, and EACA (EA with CA treatment). The IOSA and VSA results are in fair agreement, but there are significant discrepancies with the EACA cross sections. The application of the centroid approximation to the cross sections computed with EA, which neglects vibrational motion in the scattering dynamics, is clearly inadequate. EACA always peaks at $v' = 2$ and has a distribution which is too broad compared to the IOSA and VSA calculations. No experimental vibrationally-resolved data are available for this system, but similar discrepancies were noted for the $C^{2+} + H_2$ [50] and $C^{4+} + H_2$ [43] systems with SCMO calculations.

It should be noted that the current calculations do not consider the dissociation channel (i.e., $O^{2+} + H + H^+$). By definition, all two-electron transfer processes, TDC, TI, and ADC, result in dissociation (i.e., $H^+ + H^+$), but in principle, SEC can contain both nondissociative and dissociative components which may or may not be resolvable in an experiment. The current calculations demonstrate that for the $O^{3+} + H_2$ collision system that the vibrationally-resolved cross sections generally decrease with increasing vibrational num-

ber v' , relatively independent of energy. This is due to the increase in crossing distance with v' , i.e., the diabaticity of the collision increases with v' . For the $2p3s\ ^1P^o$ and $2p3s\ ^3P^o$ exit channels, the crossings occur at ~ 11.4 and $\sim 10\ a_0$ for $v' = 0$ and ~ 19 and $\sim 15\ a_0$ for $v' = 9$, respectively. The dissociative continuum would correspond to crossings greater than ~ 25 and $\sim 19\ a_0$, respectively. As the dissociative crossings are clearly diabatic, dissociative SEC is expected to be negligible, at least at low energies and for these two exit electronic channels. While there may be some dissociative couplings at short distances, these will be endoergic and only possibly contribute at high energies. This is in marked contrast to the dissociative SEC predictions for Be^{4+} and C^{4+} collisions with H_2 obtained by Errea *et al.* [32, 43] which increase with decreasing collision energy being only a factor of ~ 2 smaller than nondissociative SEC by 50 eV/u. The semiclassical method of these authors obtains the total (dissociative and nondissociative) SEC probability through a closure relation of all of the vibrational exit channels. This procedure removes the dependence on the exit vibrational wave functions and, more importantly, all dependence on the energy asymptotics. The findings in this work and the discussion above point to the importance of this latter issue. Therefore, the method of Ref. [32] is probably not appropriate for predictions of dissociative SEC at low energy. Experimental guidance is needed in this matter.

D. Rate Coefficients

We present in Fig. 14 total and ESS thermal rate coefficients as a function of collision temperature. The rate coefficients were obtained by averaging the IOSA cross sections over a Maxwellian relative velocity distribution. The results are consistent with the available ion-loss measurement of Church and Holzscheiter [25] at ~ 1500 K. The measurements are somewhat larger than the current SEC calculations, but as discussed above they are likely to contain significant contributions due to ADC and TDC.

V. SUMMARY

Quantum-mechanical molecular-orbital calculations have been presented for electron capture following O^{3+} collisions with H_2 over the energy range from 0.1 eV/u to 10 keV/u. Total, electronic state-selective, and vibrationally-resolved cross sections are presented using

the infinite order sudden approximation (IOSA) and the vibrational sudden approximation (VSA), the latter introducing vibrational motion by including Franck-Condon like factors in the radial couplings. An electronic approximation (EA) was also used with vibrationally-resolved cross sections obtained with the centroid approximation (CA). Comparison with the existing experimental data shows the IOSA and VSA total cross sections to be in agreement with previous experimental results, but less so with the recent measurement of Okuno *et al.* [27]. The electronic state-selective cross sections and the ratio of triplet and singlet cross sections obtained with IOSA and VSA are in harmony with the measurements of Beijers *et al.* [26] if allowance is given for metastable contamination. Agreement of the EA results with experiment is generally poor in all cases. Concerning vibrational distributions, there is fair agreement between IOSA and VSA, but EACA is found to be unreliable at all energies. If vibrationally-resolved information is desired, account of the vibrational motion must be included in the collision dynamics.

Acknowledgments

J G W and P C S acknowledge support from NASA grant NAG5-11453. We thank Bernard Zygelman for use of his ion-atom MO close-coupling code which formed the core of the current implementation. Thanks also to Philippe Weck for providing the H₂ and H₂⁺ vibrational wave functions and the referee for a critical reading of the manuscript.

-
- [1] S. Lepp and R. McCray, *Astrophys. J.* **269**, 560 (1983).
 - [2] S. Tiné, S. Lepp, R. Gredel, and A. Dalgarno, *Astrophys. J.* **481**, 282 (1997).
 - [3] A. Sternberg, M. Yan, and A. Dalgarno, in *Molecules in astrophysics: probes and processes*, IAU symposium 178, ed. E. F. van Dishoeck (IAU, 1996), p. 141.
 - [4] R. K. Janev, in *Atomic and Molecular Processes in Fusion Edge Plasmas*, ed. R. K. Janev (Plenum Press, New York, 1995) p. 1.
 - [5] A. Owens, A. N. Parmar, T. Oosterbroek, A. Orr, L. A. Antonelli, F. Fiore, R. Schutz, G. P. Tozzi, M. C. Maccarone, and L. Piro, *Astrophys. J.* **493**, L47 (1998).
 - [6] C. M. Lisse, *et al.*, *Science* **274**, 205 (1996).

- [7] M. J. Mumma, V. A. Krasnopolsky, and M. J. Abbott, *Astrophys. J.* **491**, L125 (1997).
- [8] T. E. Cravens, *Geophys. Res. Lett.* **24**, 105 (1997).
- [9] R. M. Haberli, T. I. Gombosi, D. L. De Zeeuw, M. R. Combi, and K. G. Powell, *Science* **276**, 939 (1997).
- [10] V. A. Krasnopolsky and M. J. Mumma, *Astrophys. J.* **549**, 629 (2001).
- [11] C. M. Lisse, *et al.*, *Science* **292**, 1343 (2001).
- [12] V. A. Krasnopolsky, D. J. Christian, V. Kharchenko, A. Dalgarno, S. Wolk, C. M. Lisse, and S. A. Stern, *Icarus* **160**, 437 (2002).
- [13] T. E. Cravens, E. Howell, J. H. Waite, Jr., and G. R. Gladstone, *J. Geophys. Res. A* **100**, 17,153 (1995).
- [14] W. Liu and D. R. Schultz, *Astrophys. J.* **530**, 500 (2000).
- [15] D. Elizaga, *et al.*, *J. Phys. B* **32**, 857 (1999).
- [16] M. C. Bacchus-Montabonel, *Phys. Rev. A* **59**, 3569 (1999).
- [17] L. F. Errea, A. Macías, L. Méndez, and A. Riera, *J. Phys. B* **32**, 4065 (1999).
- [18] L. F. Errea, J. D. Gorfinkiel, A. Macías, L. Méndez, and A. Riera, *J. Phys. B* **32**, 1705 (1999).
- [19] P. C. Stancil, B. Zygelman, and K. Kirby, *XX International Conference on the Physics of Electronic and Atomic Collisions*, ed. F. Aumayr, G. Betz, and HP. Winter (World Scientific, Singapore, 1998), p. 537.
- [20] D. H. Crandall, M. L. Mallory, and D. C. Kocher, *Phys. Rev. A* **15**, 61 (1977).
- [21] R. A. Phaneuf, F. W. Meyer, and R. H. McKnight, *Phys. Rev. A* **17**, 534 (1978).
- [22] F. W. Meyer, R. A. Phaneuf, H. J. Kim, P. Hvelplund, and P. H. Stelson, *Phys. Rev. A* **19**, 515 (1979).
- [23] R. A. Phaneuf, I. Alvarez, F. W. Meyer, and D. H. Crandall, *Phys. Rev. A* **26**, 1892 (1982).
- [24] V. V. Afrosimov, A. A. Basalaev, E. D. Donets, and M. N. Panov, *Sov. Phys.-JETP Lett.* **31**, 600 (1980).
- [25] D. A. Church and H. M. Holzscheiter, *Phys. Rev. A* **40**, 54 (1989).
- [26] J. P. M. Beijers, R. Hoekstra, and R. Morgenstern, *J. Phys. B: At. Mol. Opt. Phys.* **29**, 1397 (1996).
- [27] K. Okuno, *et al.*, private communication (2002).
- [28] D. L. Cooper, N. J. Clarke, P. C. Stancil, and B. Zygelman, *Adv. Quant. Chem.* **40**, 37 (2001).
- [29] A. R. Turner, *Doctoral Thesis*, University of Liverpool (2002).

- [30] NIST Atomic Spectra Database, Version 2.0, 1999. <http://physics.nist.gov/asd> .
- [31] J. G. Wang, P. C. Stancil, A. R. Turner, and D. L. Cooper, *Phys. Rev. A* **67**, 012710 (2003).
- [32] L. F. Errea, J. D. Gorfinkiel, E. S. Kryachko, A. Macías, L. Méndez, and A. Riera, *J. Chem. Phys.* **106**, 172 (1997).
- [33] M. Kimura and N. F. Lane, *Ad. At. Mol. Phys.* **26**, 79 (1990).
- [34] B. Zygelman, D. L. Cooper, M. J. Ford, A. Dalgarno, J. Gerratt, and M. Raimondi, *Phys. Rev. A* **46**, 3846 (1992).
- [35] V. Sidis, *Adv. At. Mol. Phys.* **26**, 161 (1989).
- [36] M. Kimura, J.-P. Gu, G. Hirsch, R. J. Buenker, and P. C. Stancil, *Phys. Rev. A* **61**, 032708 (2000).
- [37] M. Gargaud and R. McCarroll, *J. Phys. B: At. Mol. Opt. Phys.* **18**, 463 (1985).
- [38] M. Kimura and N. F. Lane, *Phys. Rev. A* **35**, 70 (1985).
- [39] B. C. Saha, N. F. Lane, and M. Kimura, *Phys. Rev. A* **44**, R1 (1991).
- [40] S. Kravis, *et al.*, *Phys. Rev. A* **52**, 1206 (1995).
- [41] T. G. Heil, S. E. Butler, and A. Dalgarno, *Phys. Rev. A* **27**, 2365 (1983).
- [42] L. F. Errea, *et al.*, *Physica Scripta* **T62**, 33 (1996).
- [43] L. F. Errea, J. D. Gorfinkiel, A. Macías, L. Méndez, and A. Riera, *J. Phys. B: At. Mol. Opt. Phys.* **32**, 4065 (1999).
- [44] R. K. Janev, R. A. Phaneuf, and H. T. Hunter, *Atom. Data Nucl. Data Tables* **40**, 249 (1988).
- [45] J. G. Wang, M. J. Raković, D. R. Schultz, and P. C. Stancil, in preparation (2003).
- [46] W. L. Wiese, J. R. Fuhr, and T. M. Deters, *J. Phys. Chem. Reference Data Monograph No.* 7 (1996).
- [47] P. Beiersdorfer, C. M. Lisse, R. E. Olson, G. V. Brown, and H. Chen, *Astrophys. J.* **549**, L147 (2001).
- [48] B. J. Wargelin and J. J. Drake, *Astrophys. J.* **546**, L57 (2001).
- [49] V. Kharchenko and A. Dalgarno, *Astrophys. J.* **554**, L99 (2001).
- [50] L. F. Errea, A. Macías, L. Méndez, I. Rabadán, and A. Riera, *J. Phys. B* **33** L615 (2000).
- [51] Complete numerical cross section and rate coefficient data can be obtained from the authors or from the ORNL-UGA Charge Transfer Database for Astrophysics webpage (URL: cfadc.phy.ornl.gov/astro/ps/data).

TABLE I: Virtuals selected for SCVB expansions for OH_2^{3+} (listed according to asymptotic characters).

Stack				
1	2	3	4	5
$\text{O}^{2+}(3s)$	$\text{H}_2(2\sigma_g)$	$\text{O}^{2+}(3p_x)$	$\text{O}^{2+}(3s)$	$\text{O}^{2+}(2p_y)$
$\text{O}^{2+}(3d_0)$	$\text{H}_2(3\sigma_g)$	$\text{H}_2^+(1\sigma_g)$	$\text{O}^{2+}(3p_x)$	$\text{O}^{2+}(3p_y)$
			$\text{H}_2^+(1\sigma_g)$	
$\text{O}^{2+}(2p_y)$		$\text{O}^{2+}(2p_y)$	$\text{O}^{2+}(2p_y)$	
$\text{O}^{2+}(3p_y)$		$\text{O}^{2+}(4p_y)$	$\text{O}^{2+}(3p_y)$	
			$\text{O}^{2+}(3d_{2+})$	

TABLE II: Asymptotic separated-atom energies for the states of OH_2^{3+} .

Molecular States	Asymptotic Atomic states	Energy (eV)	
		Theory ^a	Expt ^b
1 $^2A'$	$\text{O}^{2+}(2s^22p3s \ ^3P^o)+\text{H}_2^+(X \ ^2\Sigma_g^+)$	-5.33	-5.33
2 $^2A'$	$\text{O}^{2+}(2s^22p3s \ ^1P^o)+\text{H}_2^+(X \ ^2\Sigma_g^+)$	-4.61	-4.64
-	$\text{O}^{2+}(2s^22p3p \ ^1P)+\text{H}_2^+(X \ ^2\Sigma_g^+)$	-2.45	-2.42
-	$\text{O}^{2+}(2s^22p3p \ ^3D)+\text{H}_2^+(X \ ^2\Sigma_g^+)$	-2.00	-2.04
-	$\text{O}^{2+}(2s^22p3p \ ^3S)+\text{H}_2^+(X \ ^2\Sigma_g^+)$	-1.71	-1.61
-	$\text{O}^{2+}(2s^22p3p \ ^3P)+\text{H}_2^+(X \ ^2\Sigma_g^+)$	-1.37	-1.26
3 $^2A'$	$\text{O}^{3+}(2s^22p \ ^2P^o)+\text{H}_2(X \ ^1\Sigma_g^+)$	1.07	0.0

^aThis work for $\theta = 89^\circ$ and an H-H bond length $r = 1.4 a_0$ with the energies shifted to match experiment for the 1 $^2A'$.

^bThe oxygen energies are taken from the NIST Atomic Spectra Database [30]. The adopted H_2 vertical ionization energy, for $r = 1.4 a_0$, is taken to be 132613.1 cm^{-1} .

TABLE III: Avoided crossing distances and energy separations for the adiabatic states of OH_2^{3+} (adiabatic labels).

$\theta(^{\circ})$	$r(a_0)$	Molecular		ΔU (eV)
		States	$R_x(a_0)$	
25.0	1.4	$1^2A' - 2^2A'$	8.72	0.330
		$2^2A' - 3^2A'$	9.56	0.109
45.0	1.2	$1^2A' - 2^2A'$	9.84	0.050
		$2^2A' - 3^2A'$	11.22	0.041
	1.4	$1^2A' - 2^2A'$	8.76	0.338
		$2^2A' - 3^2A'$	9.56	0.101
	1.6	$1^2A' - 2^2A'$	8.12	0.532
		$2^2A' - 3^2A'$	8.54	0.230
89.0	1.2	$1^2A' - 2^2A'$	9.95	0.118
		$2^2A' - 3^2A'$	11.31	0.033
	1.4	$1^2A' - 2^2A'$	8.70	0.289
		$2^2A' - 3^2A'$	9.56	0.074
	1.6	$1^2A' - 2^2A'$	7.93	0.485
		$2^2A' - 3^2A'$	8.43	0.225
	2.0	$1^2A' - 2^2A'$	8.00	0.682
		$2^2A' - 3^2A'$	7.50	0.670

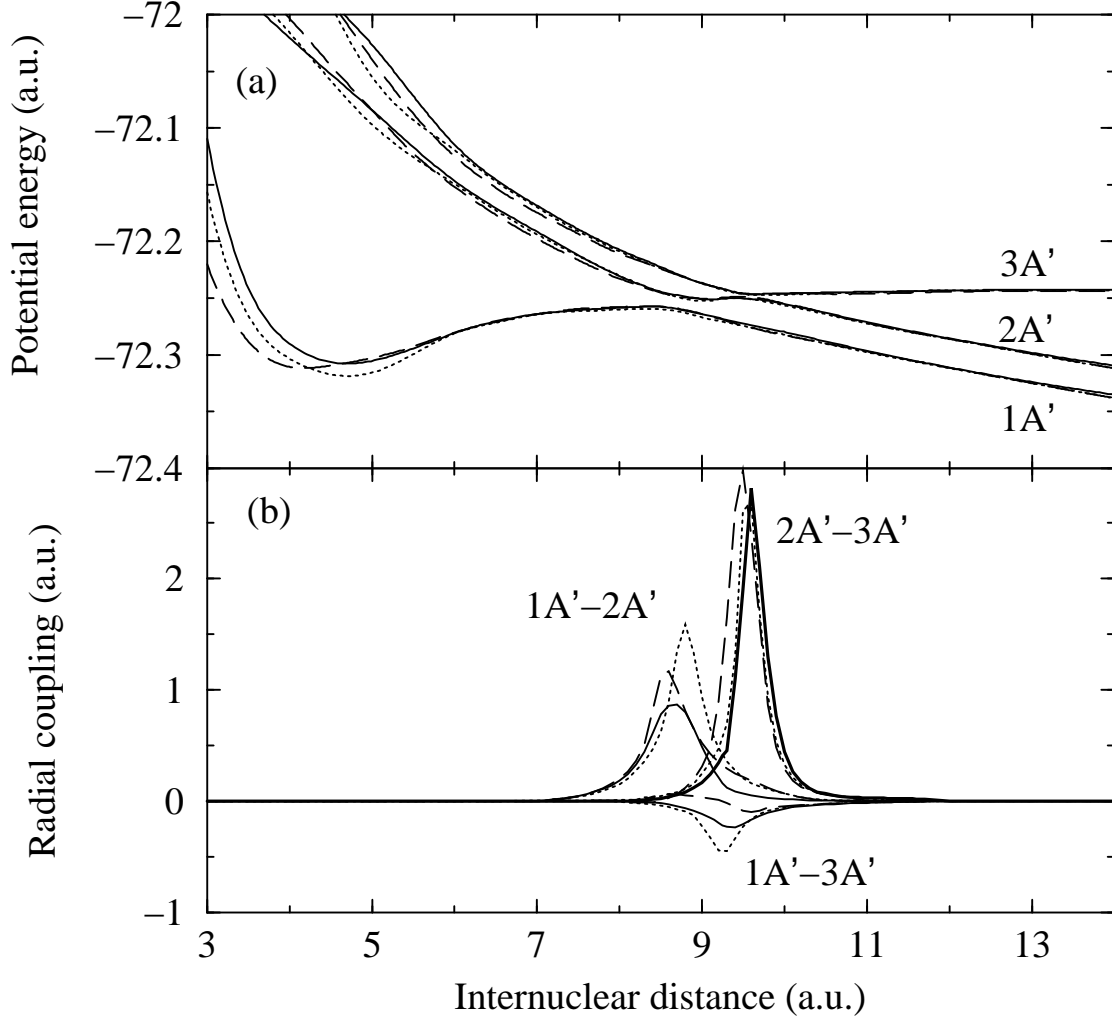


FIG. 1: The adiabatic potential curves and radial couplings for OH_2^+ as a function of R with r held fixed at $1.4a_0$. Solid curves: $\theta = 25^\circ$, dotted curves: $\theta = 45^\circ$, and long dashed curves: $\theta = 89^\circ$. (a) The potentials: the uppermost curves separate to $\text{O}^{3+}(2s^22p^2P^o) + \text{H}_2(X^1\Sigma_g^+)$, the middle curves to $\text{O}^{2+}(2p3s^1P^o) + \text{H}_2^+(X^2\Sigma_g^+)$ and the lower curves to $\text{O}^{2+}(2p3s^3P^o) + \text{H}_2^+(X^2\Sigma_g^+)$. (b) The radial couplings: The outermost couplings corresponding to $2A' - 3A'$, the middle couplings to $1A' - 3A'$, and the innermost couplings corresponding to $1A' - 2A'$.

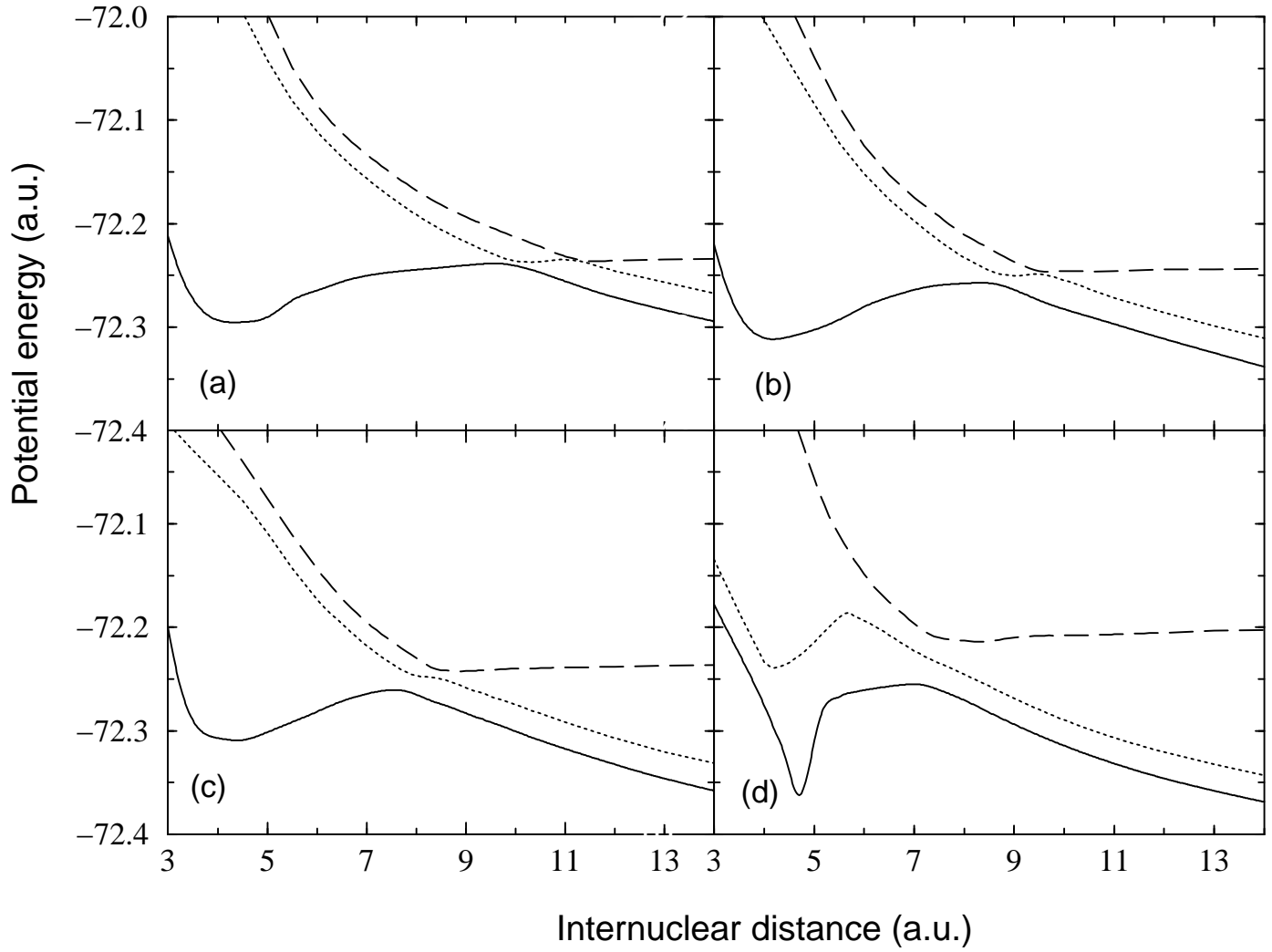


FIG. 2: The adiabatic potential curves for OH_2^{3+} as a function of R held fixed at $\theta = 89^\circ$. (a) $r = 1.2a_0$, (b) $r = 1.4a_0$, (c) $r = 1.6a_0$, and (d) $r = 2.0a_0$.

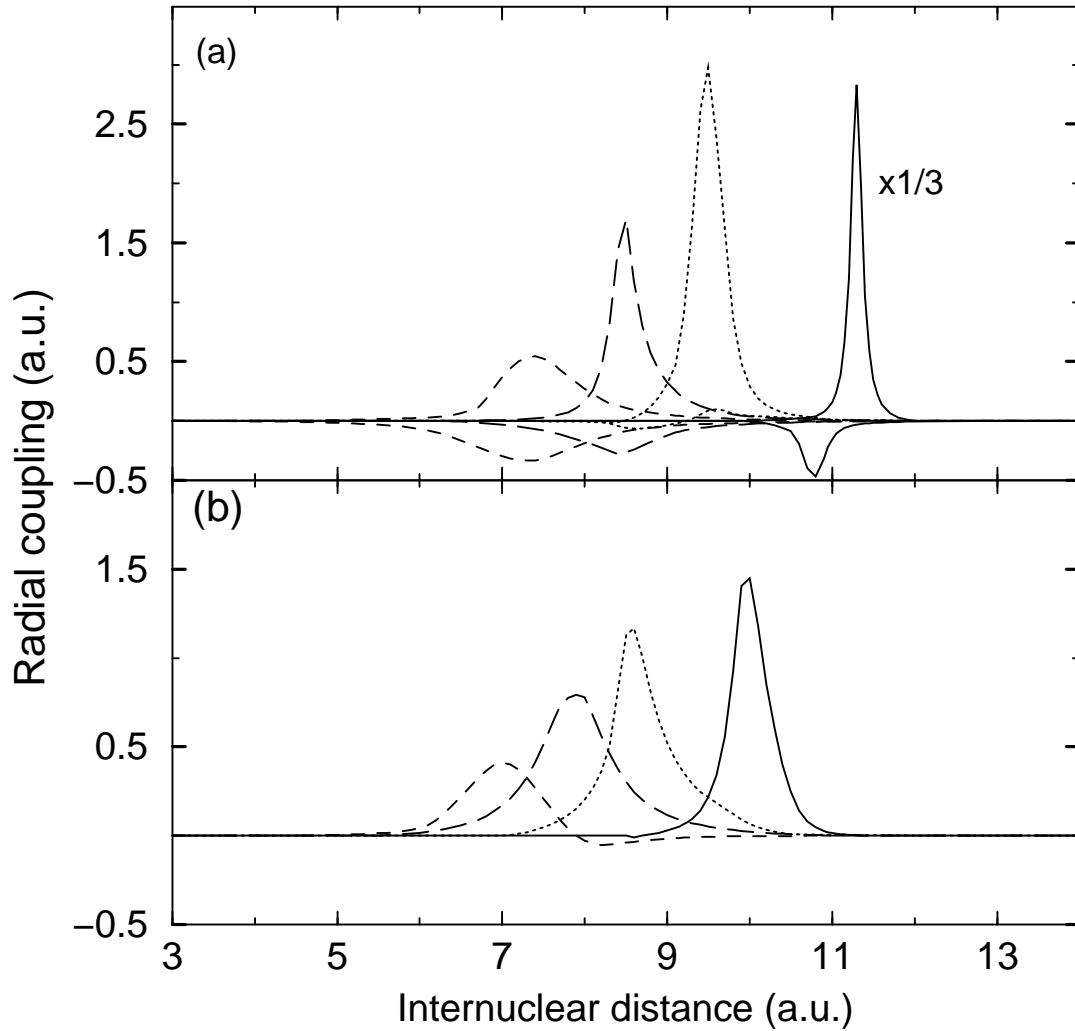


FIG. 3: The adiabatic radial couplings for OH_2^{3+} as a function of R held fixed at $\theta = 89^\circ$. Solid curves: $r = 1.2a_0$, dotted curves: $r = 1.4a_0$, long dashed curves: $r = 1.6a_0$, and short dashed curves: $r = 2.0a_0$. (a) $2A' - 3A'$ couplings upper and $1A' - 3A'$ couplings lower. (b) $1A' - 2A'$ couplings.

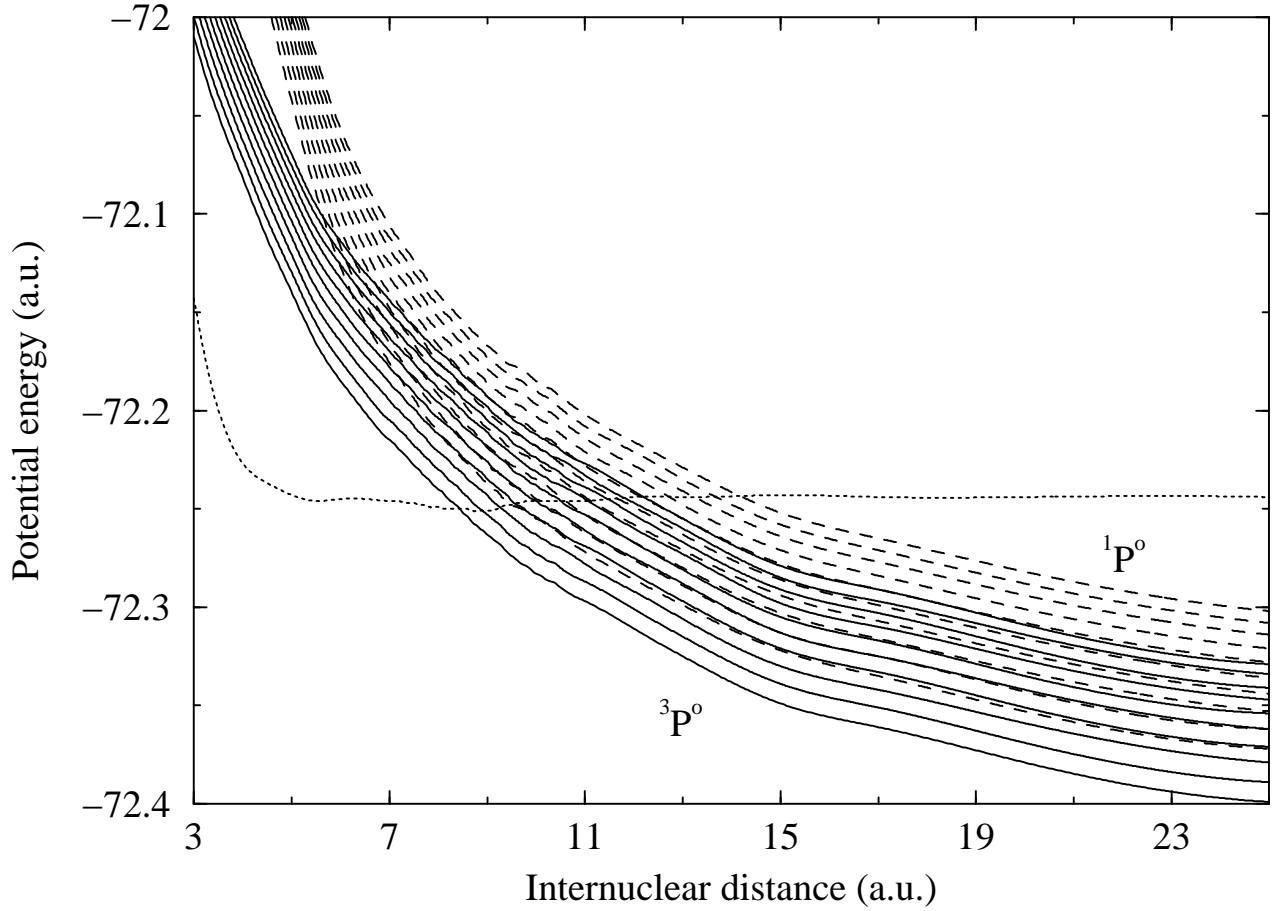


FIG. 4: The diabatic vibronic potential curves for OH_2^{3+} as a function of R for $\theta = 89^\circ$. Solid curves from lower to higher separate to $\text{O}^{2+}(2p3s\ ^3P^o) + \text{H}_2^+(X\ ^2\Sigma_g^+, v')$ from $v' = 0$ to $v' = 9$. Dashed curves from lower to higher separate to $\text{O}^{2+}(2p3s\ ^1P^o) + \text{H}_2^+(X\ ^2\Sigma_g^+, v')$ from $v' = 0$ to $v' = 9$. Dotted curve separates to $\text{O}^{3+}(2s^22p\ ^2P^o) + \text{H}_2(X\ ^1\Sigma_g^+, v = 0)$.

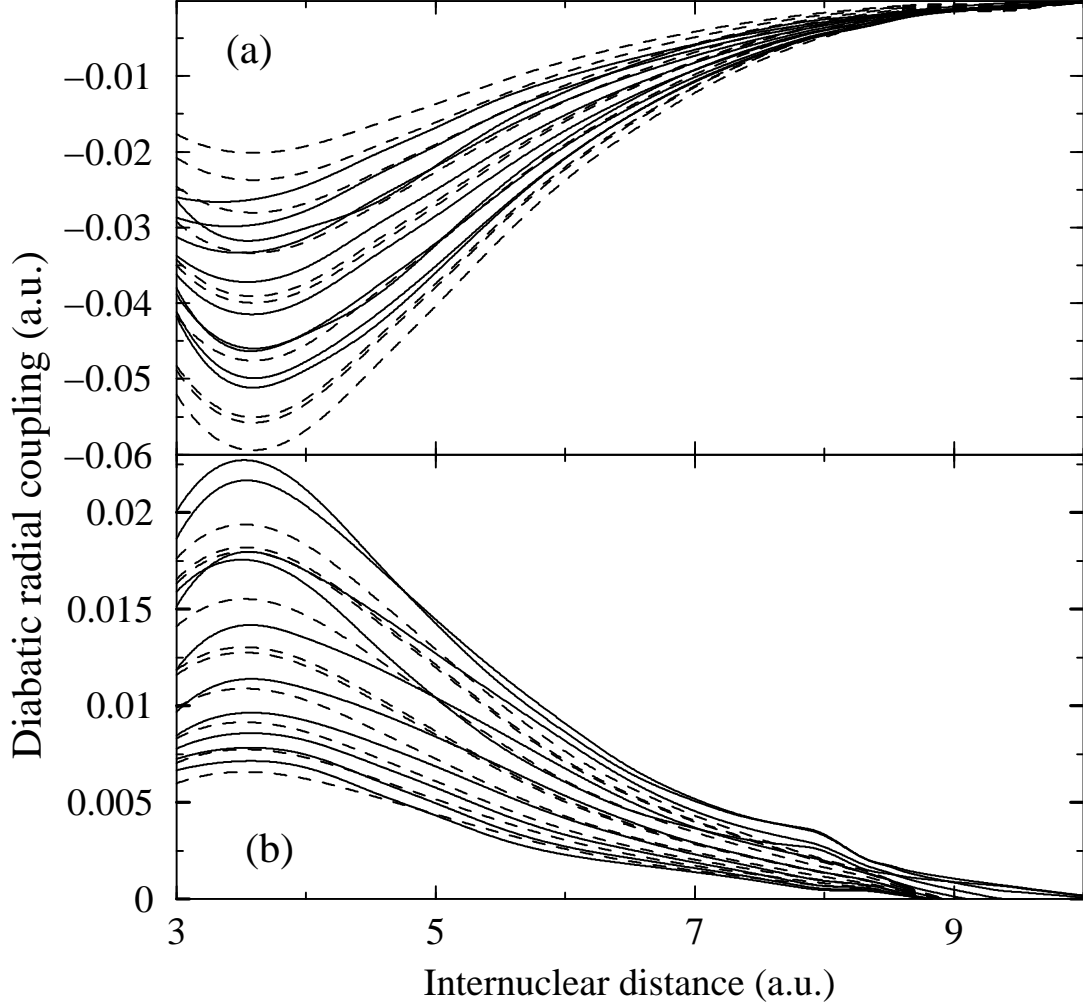


FIG. 5: The diabatic vibronic radial couplings for OH_2^{3+} as a function of R for $\theta = 89^\circ$. (a) Capture to $\text{O}^{2+}(2p3s\ ^3P^o) + \text{H}_2^+(X\ ^2\Sigma_g^+, v' = 0 - 9)$: Solid curves (IOSA) from bottom to top at $R = 4a_0$ correspond to $v' = 2, 3, 4, 1, 5, 6, 7, 0, 8, 9$. Dashed curves (VSA) from bottom to top at $R = 4a_0$ correspond to $v' = 2, 1, 3, 4, 0, 5, 6, 7, 8, 9$. (b). Capture to $\text{O}^{2+}(2p3s\ ^1P^o) + \text{H}_2^+(X\ ^2\Sigma_g^+, v' = 0 - 9)$. Solid curves (IOSA) from top to bottom at $R = 4a_0$ correspond to $v' = 1, 2, 0, 3, 4, 5, 6, 7, 8, 9$. Dashed curves (VSA) from top to bottom at $R = 4a_0$ correspond to $v' = 2, 1, 3, 4, 0, 5, 6, 7, 8, 9$.

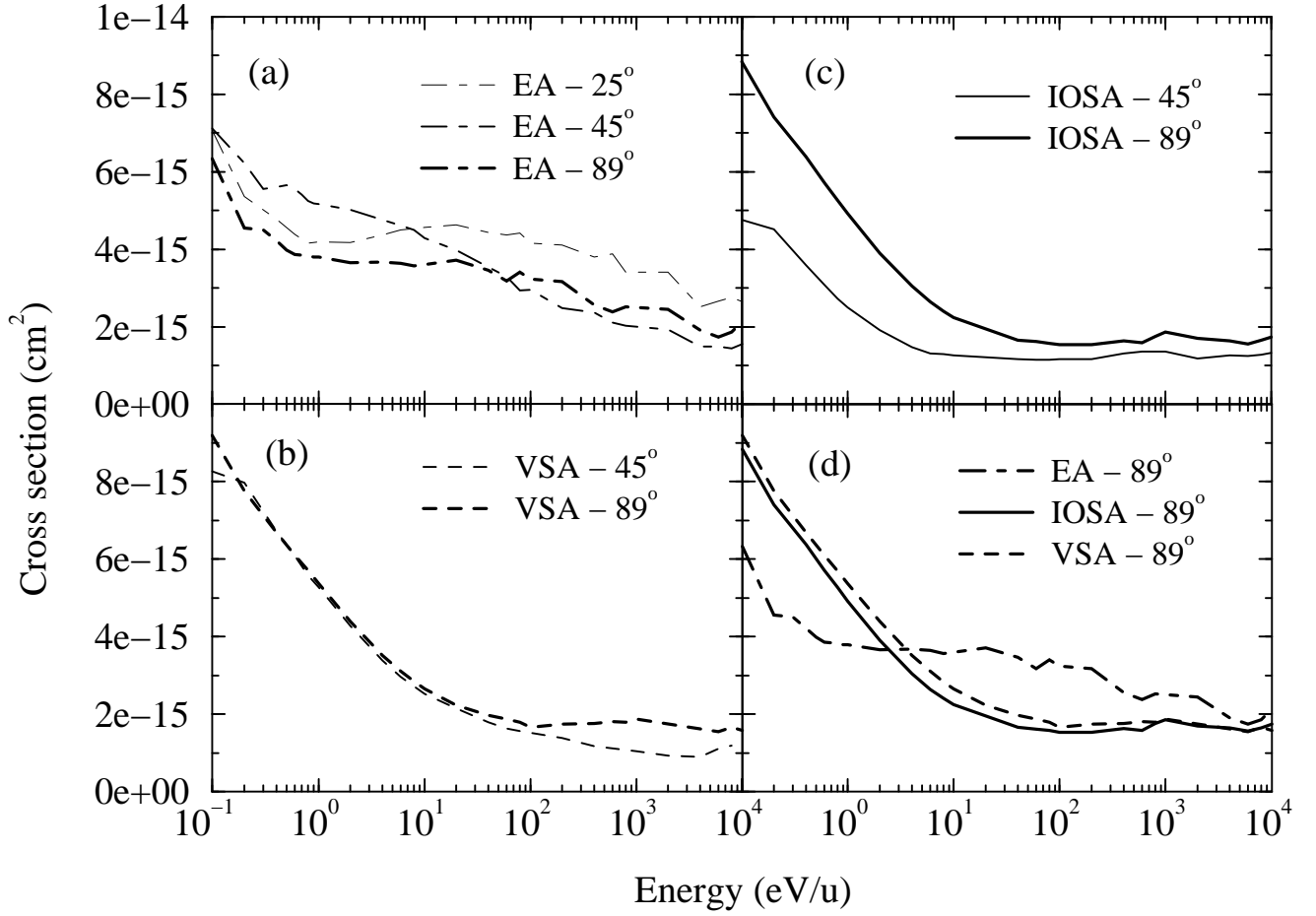


FIG. 6: Orientation-dependent total SEC cross sections for $O^{3+} + H_2$. (a) EA (dot-dashed lines) (b) VSA (dashed lines), (c) IOSA (full lines), and and EA (dot-dashed lines) for $\theta = 25^\circ$ (EA only), $\theta = 45^\circ$, and $\theta = 89^\circ$. (d) Comparison of EA, IOSA, and VSA for $\theta = 89^\circ$.

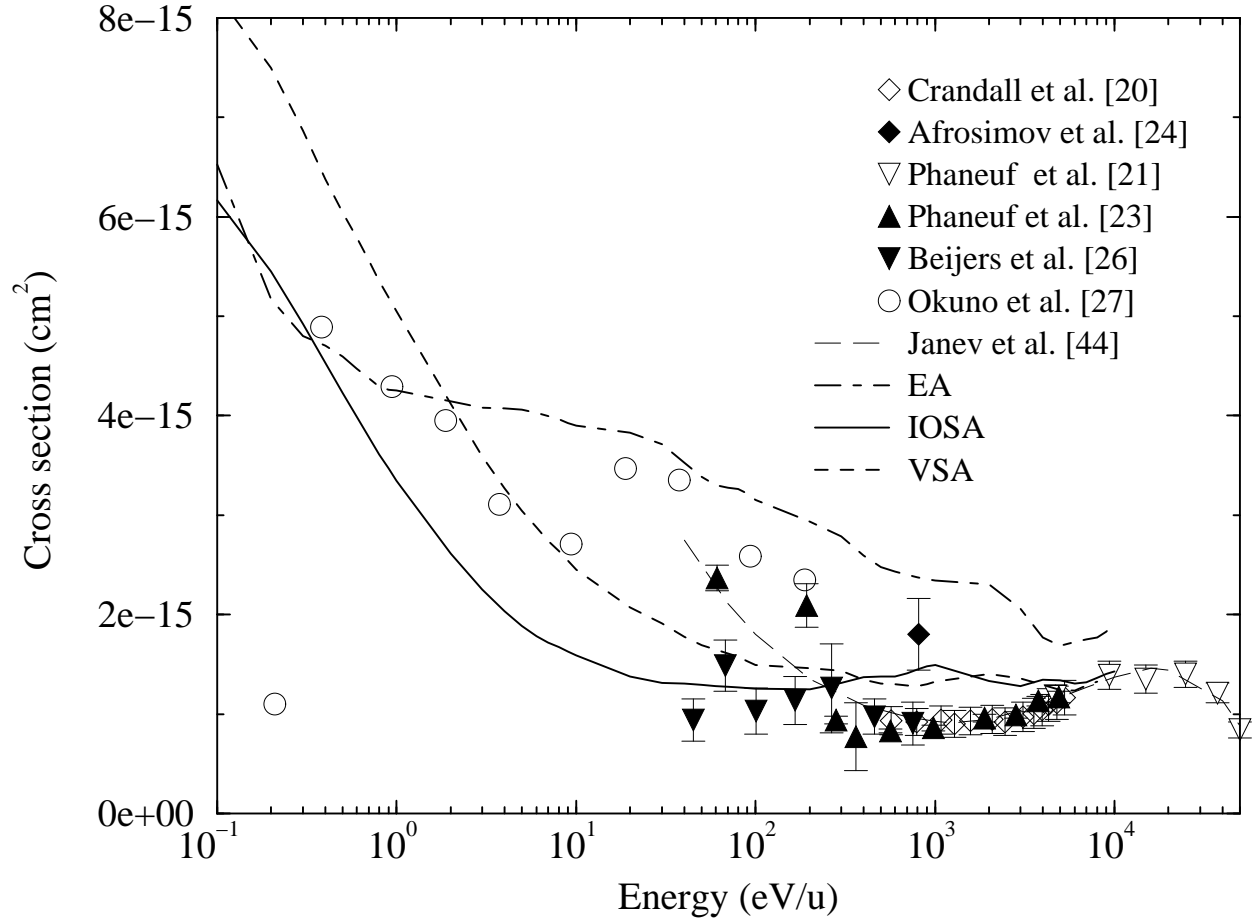


FIG. 7: Orientation-averaged total cross sections for $O^{3+} + H_2$. Theory: EA (thick dash-dot curve), IOSA (thick solid curve), VSA (thick dashed curve). Recommendation: Janev *et al.* [44] (thin long-dashed curve). Experiment: Crandall *et al.* [20] (open diamonds), Afrosimov *et al.* [24] (filled diamonds), Phaneuf *et al.* [21] (open triangles down), Phaneuf *et al.* [23] (filled triangles up), Beijers *et al.* [26] (filled triangles down), Okuno *et al.* [27] (open circles).

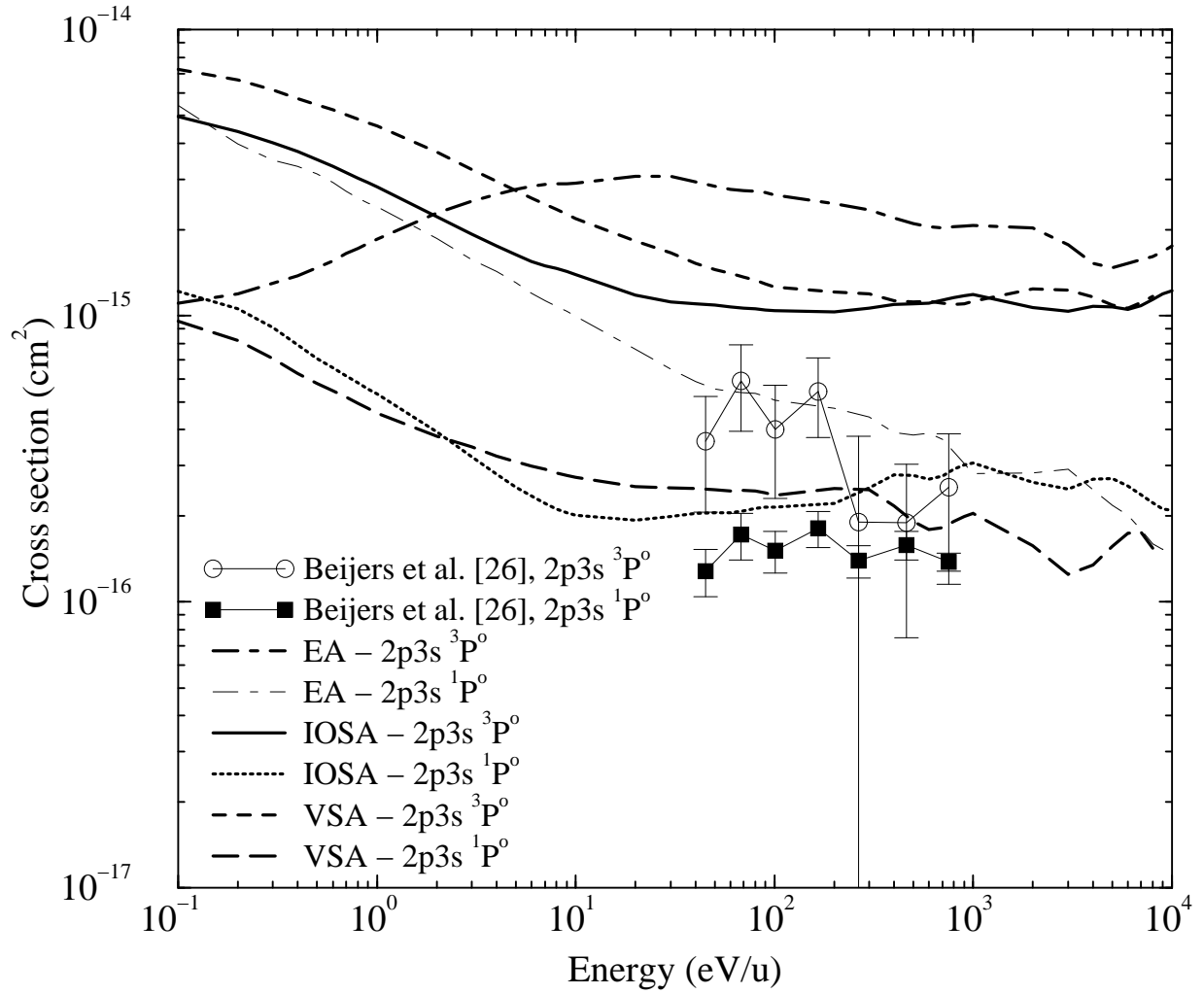


FIG. 8: Electronic state-selective cross sections for $O^{3+} + H_2$. Theory: EA, $O^{2+}(2p3s \ ^3P^o)$ (thick dash-dot curve) and $O^{2+}(2p3s \ ^1P^o)$ (thin dash-dot curve); IOSA, $O^{2+}(2p3s \ ^3P^o)$ (thick solid curve) and $O^{2+}(2p3s \ ^1P^o)$ (thick dotted curve), and VSA, $O^{2+}(2p3s \ ^3P^o)$ (thick dashed curve) and $O^{2+}(2p3s \ ^1P^o)$ (thick long-dashed curve). Experiment: Beijers *et al.* [26] for capture to $O^{2+}(2p3s \ ^3P^o)$ (thin solid curve with open circles), $O^{2+}(2p3s \ ^1P^o)$ (thin solid curve with filled squares).

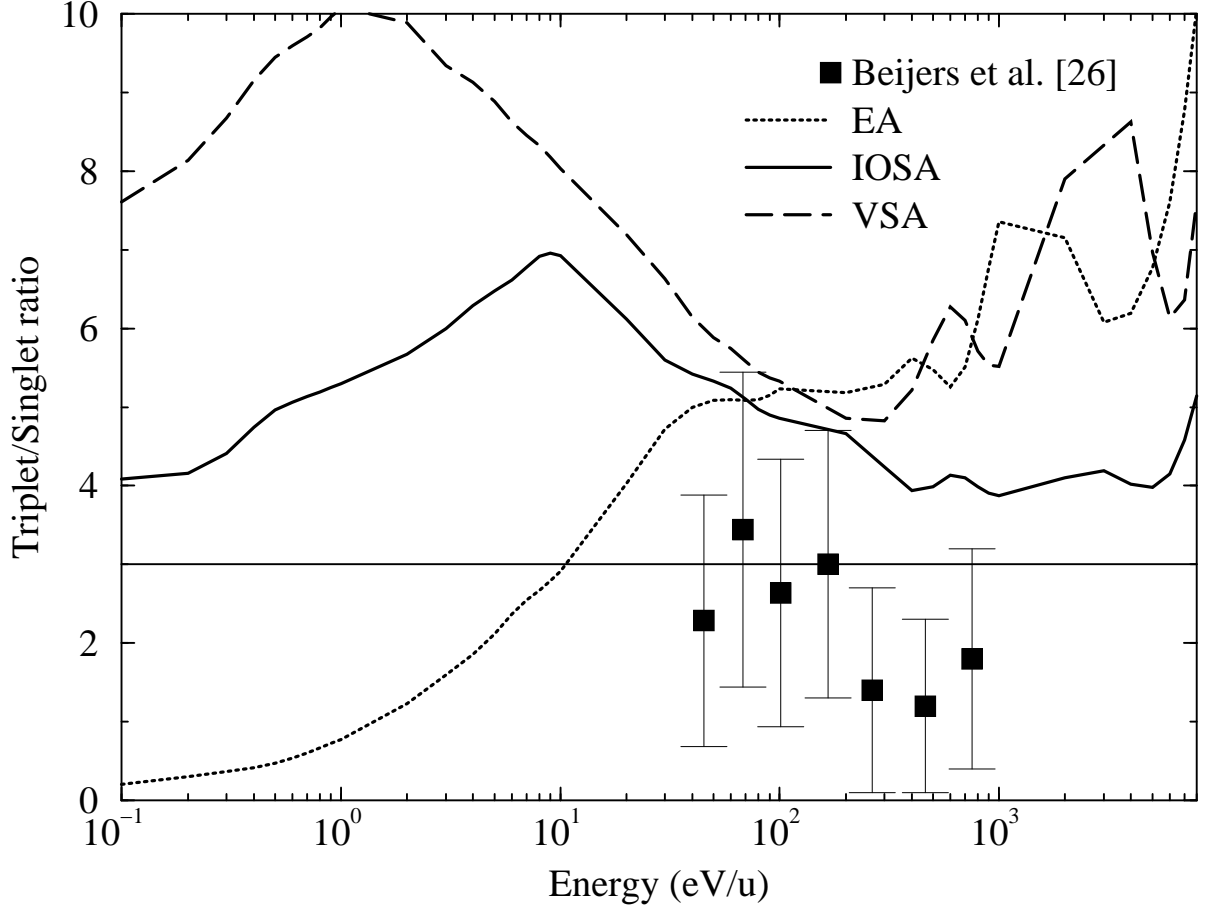


FIG. 9: The ratios of state-selective cross sections for capture to $O^{2+}(2p3s\ ^3P^o)$ and $O^{2+}(2p3s\ ^1P^o)$. Theory: EA (dotted curve), IOSA (solid curve), VSA (dashed curve). Experiment: Beijers *et al.* [26].

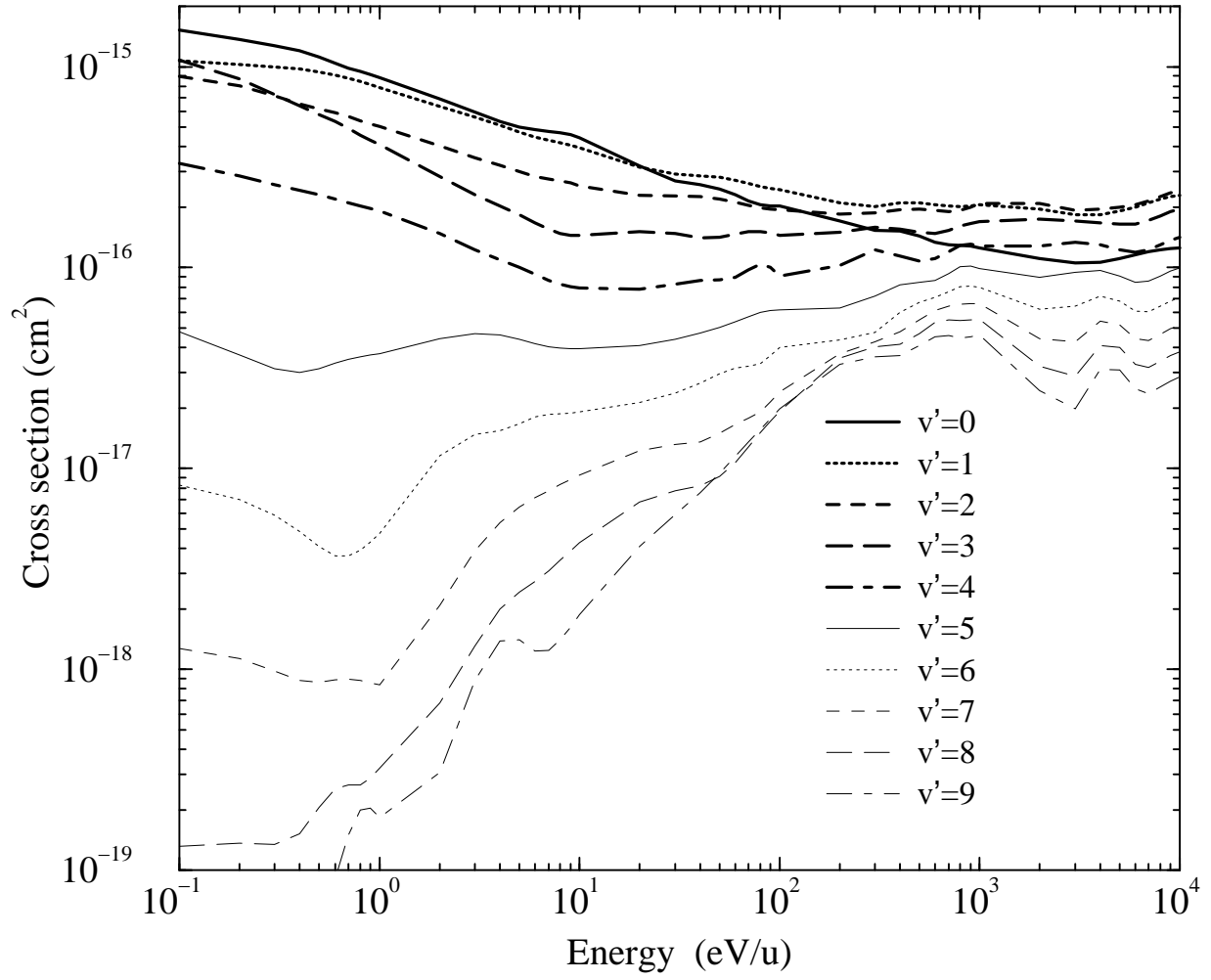


FIG. 10: Vibrationally-resolved IOSA state-selective cross sections for capture to $O^{2+}(2p3s\ ^3P^o)+H_2^+(v' = 0 - 9)$.

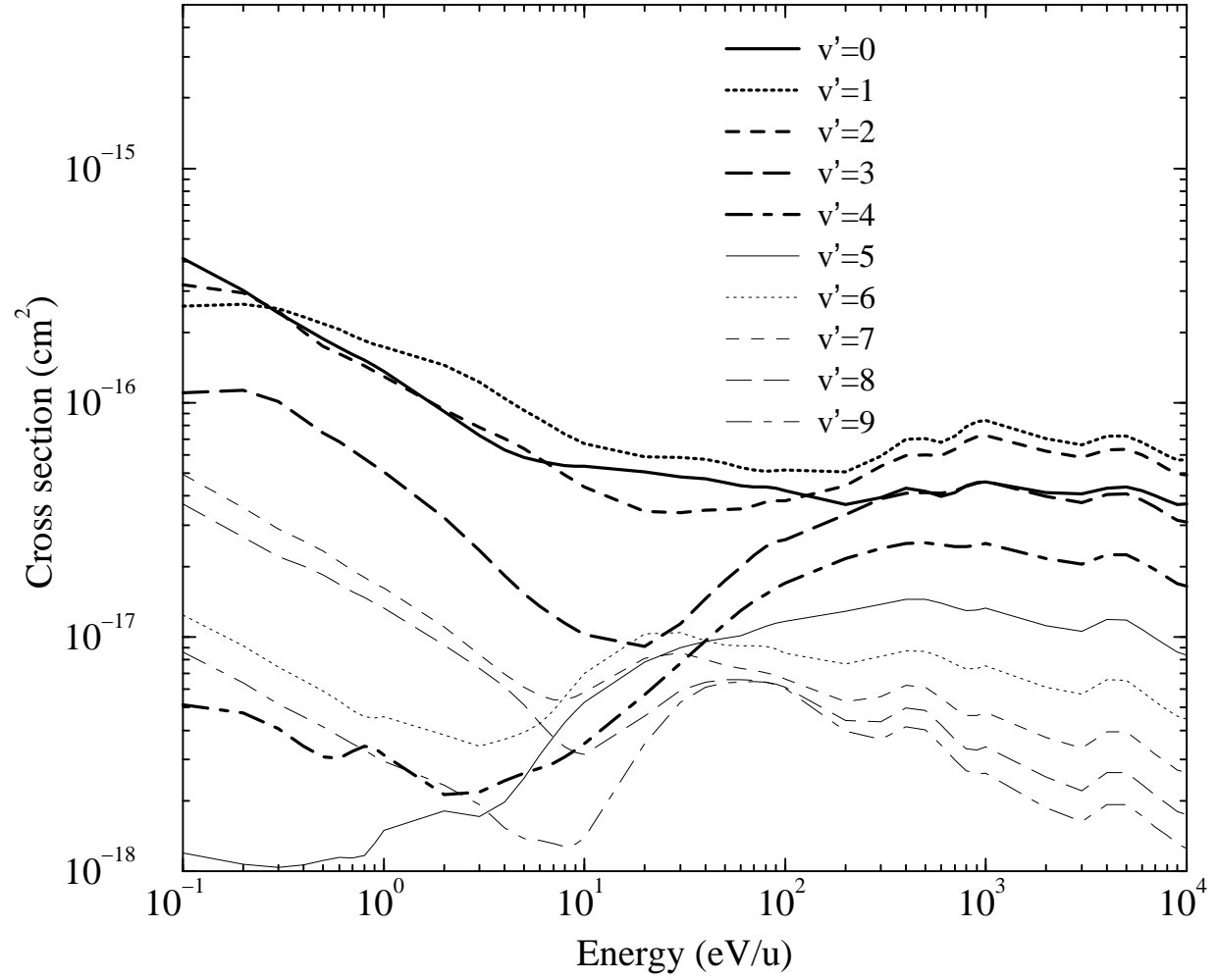


FIG. 11: Vibrationally-resolved IOSA state-selective cross sections for capture to $O^{2+}(2p3s\ ^1P^o)+H_2^+(v' = 0 - 9)$.

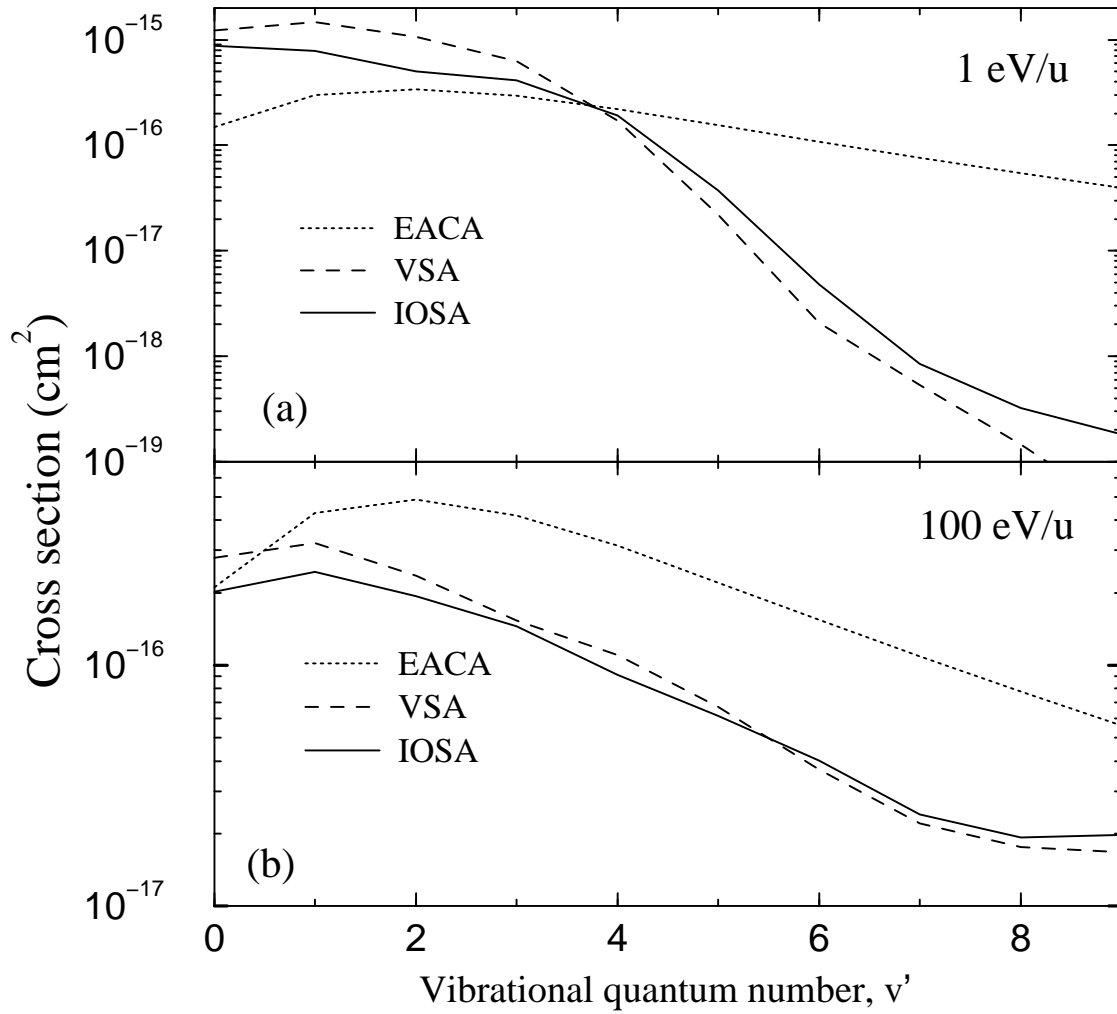


FIG. 12: Vibrationally-resolved state-selective cross sections for capture to $\text{O}^{2+}(2p3s \ ^3P^o)+\text{H}_2^+(v')$ as a function of v' at (a) 1 eV/u and (b) 100 eV/u. EACA (dotted curve), IOSA (solid curve), VSA (dashed curve).

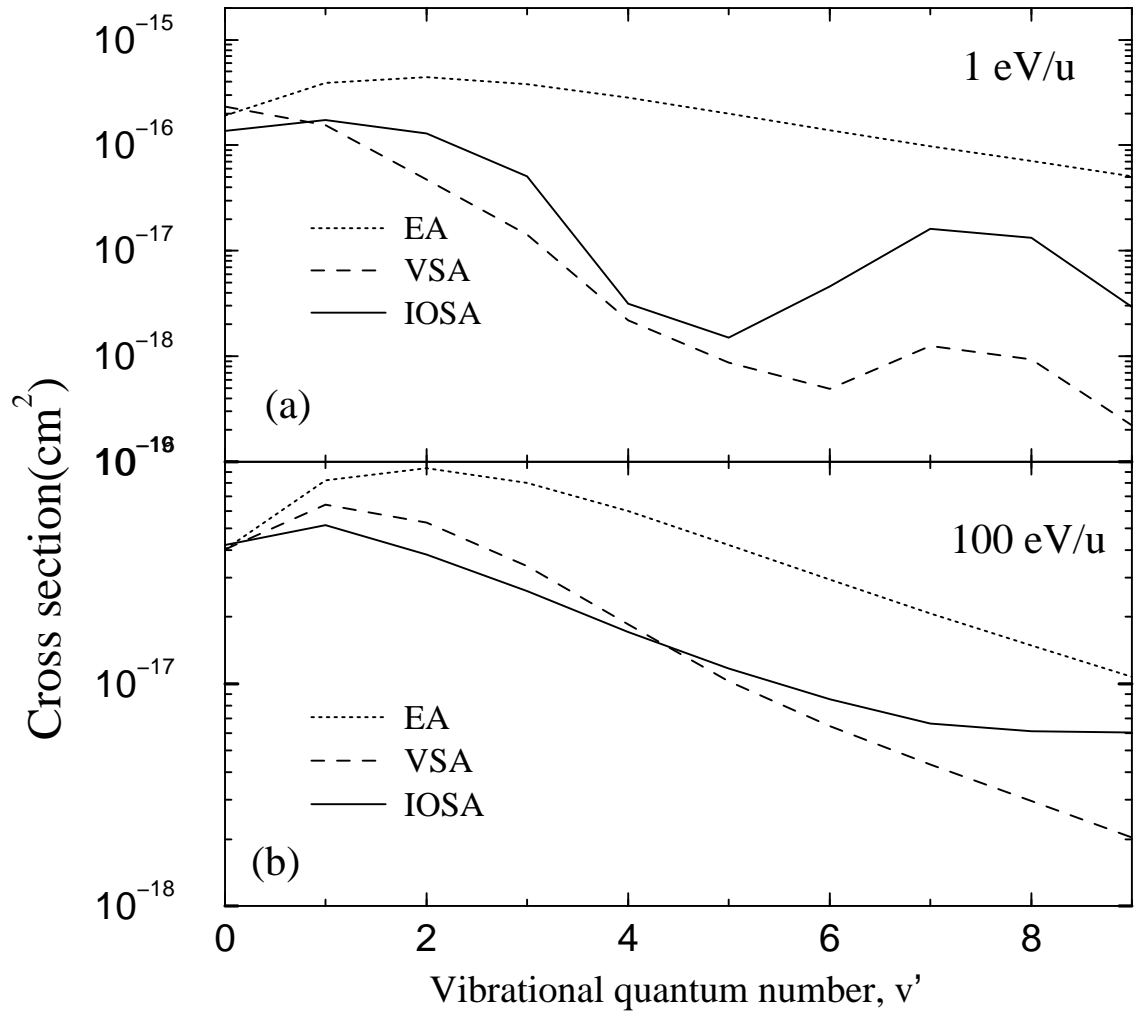


FIG. 13: Vibrationally-resolved state-selective cross sections for capture to $O^{2+}(2p3s \ ^1P^0)+H_2^+(v')$ as a function of v' at (a) 1 eV/u and (b) 100 eV/u. EACA (dotted curve), IOSA (solid curve), VSA (dashed curve).

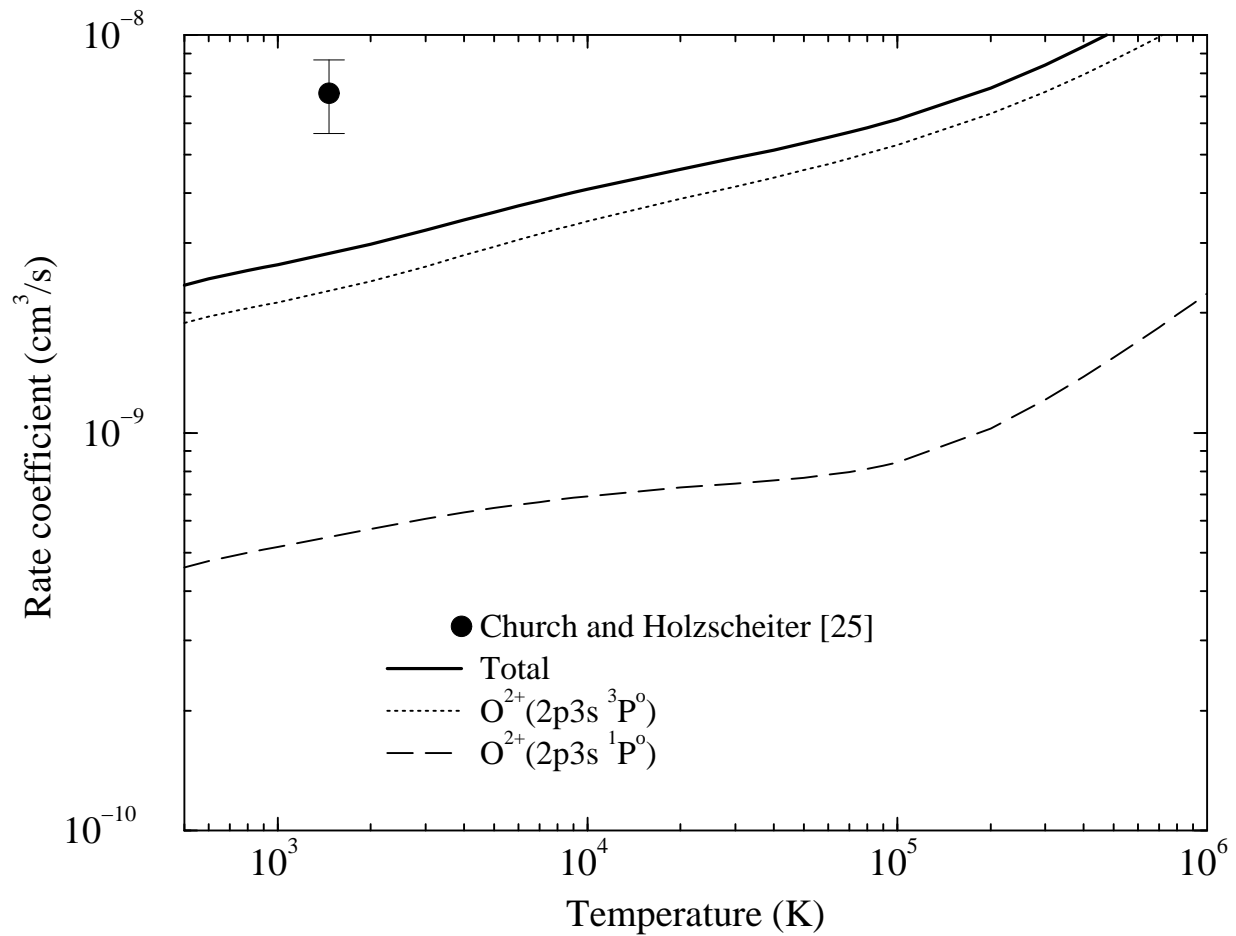


FIG. 14: Total and electronic-state-selective rate coefficients for $O^{3+} + H_2$ SEC. IOSA theory: total (solid curve), $O^{2+}(2p3s \ ^3P^o)$ (dotted curve), and $O^{2+}(2p3s \ ^1P^o)$ (dashed curve). Experiment: Church and Holzscheiter [25].